JOURNAL OF CHEMICAL INFORMATION AND MODELING

Article

pubs.acs.org/jcim

Dynamic Structure of NGF and proNGF Complexed with p75NTR: Pro-Peptide Effect

A. C. Pimenta,[†] D. F. A. R. Dourado,[‡] J. M. Martins,[†] A. Melo,[†] M. N. Dias Soeiro Cordeiro,[†] R. D. Almeida,[§] G. Morra,[∥] and I. S. Moreira*[,†]

[†]REQUIMTE Departamento de Química e Bioquímica, Faculdade de Ciências da Universidade do Porto, Rua do Campo Alegre s/n, 4169-007 Porto, Portugal

[‡]Department of Cell and Molecular Biology, Computational and Systems Biology, Uppsala Biomedicinska Centrum BMC, Box 596 751 24, Uppsala, Sweden

[§]CNC-Center for Neuroscience and Cell Biology, University of Coimbra, Coimbra, Portugal

[∥]Istituto di Chimica del Riconoscimento Molecolare, CNR, 20131 Milano, Milano, Italy

Weill Cornell Medical College, New York, New York 10021, United States

Supporting Information

ABSTRACT: Crystallographic structures of NGF/p75NTR and proNGF/p75NTR were previously obtained in 2:1 and 2:2 stoichiometries, respectively. However, evidence shows that both stoichiometries can occur for mature neurotrophins and pro-neurotrophins. We used Molecular Dynamics (MD) simulations to examine the energetic and structural characteristics of these two complete systems as well as the uncomplexed forms of NGF and understand how these could translate in a new view of different biological outcomes. Here, we show that one chain at the 2:2 proNGF complex seems to be preferentially lost creating a 2:1 structure able to interact with sortilin. We also demonstrated that the structure of the neurotrophin dimers is not pre-established and suffers large structural modifications upon p75NTR binding. Moreover, our data suggests an elegant explanation for the dual role of NGF in neuronal cell death and survival, where different stoichiometries induce conformational changes that might be the basis for the different biological outcomes observed with the mature and proforms of neurotrophins.

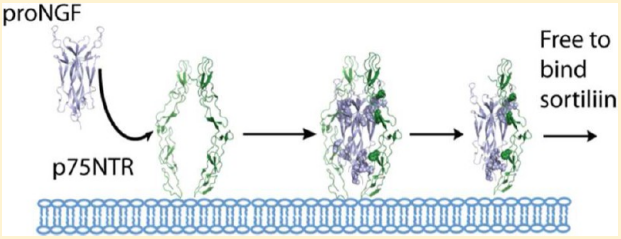

INTRODUCTION

The nerve growth factor (NGF) was the first neurotrophin to be identified and has several functions in the development and maintenance of the nervous system.[1,2] Neurotrophins exert their activity by binding to two different classes of receptors, the tropomyosin-receptor-kinase (Trk) and the p75 neurotrophin receptor (p75NTR).[3−5] NGF was initially identified as a key player in neuronal maintenance and survival of the peripheral nervous system. NGF, like other neurotrophins, is initially translated as a longer precursor, known as pre-proNGF, which contains a signal peptide for protein secretion (prepeptide).[2,6,7] This peptide is cleaved in the endoplasmic reticulum mediated by the N-terminal sequence. As a result, a 50 kDa precursor homodimer named proNGF is formed. The pro-region of NGF (103 amino acids) helps with proper folding of the protein under oxidative conditions and stabilizes the mature moiety preventing aggregation or unfolding with increasing temperatures.[7−9] The pro-sequence is then further processed in the trans-Golgi network by the protease furin at a highly conserved dibasic amino acid site and results in the release of the mature NGF dimer of 26 kDa.[4,10,11] Under certain cellular scenarios only a fraction of proNGF peptides are cleaved, which originates the secretion of both forms of NGF - mature NGF and proNGF.[11]

The crystallographic structures of these systems were attained very recently.[3,6] An asymmetrical crystal was obtained for the NGF dimer/p75NTR complex, which is characterized by two different binding sites (Sites 1 and 2 in Figure 1A).[3] The structural motif loop L2 is supposedly a key player in the asymmetry. It is hypothesized that NGF binding to p75NTR produces an allosteric effect that ultimately will lead to a structural variance in the loop and steric hindrance.[3]

More recently, proneurotrophins were shown to induce neuronal cell death,[6,12,13] by binding of the proNGF dimer to two p75NTR molecules (symmetrical complex) with posterior binding to sortilin.[6,9,14] The symmetric proNGF/p75NTR complex is similar to the asymmetrical one and presents p75NTR in the junction of the proNGF dimer. However, an extra binding site can be identified (Site 3 in Figure 1b). Although this complex was purified in the presence of the proNGF, as the pro-peptide is an IUR (Intrinsically Unfolded Region) it was not possible to obtain a tridimensional structure

Received: February 17, 2014

 © XXXX American Chemical Society dx.doi.org/10.1021/ci500101n | J. Chem. Inf. Model. XXXX, XXX, XXX−XXX

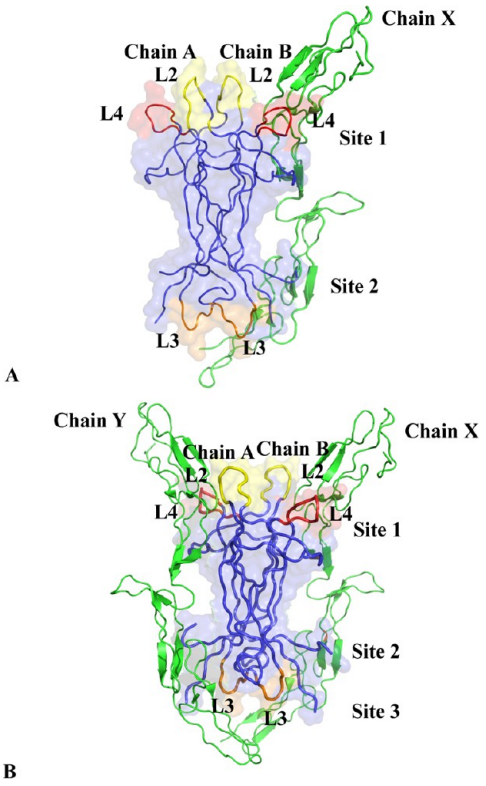

Figure 1. Structural representations of (A) NGF/p75NTR (PDBid: 1SG1[3]) and (B) proNGF/p75NTR (PDBid: 3IJ2[6]) complexes. P75NTR (Chains X and Y) is colored in green and NGF (Chains A and B) in blue. Loops L2 are highlighted in yellow, L3 in orange, and L4 in red.

of this region.[6] The disordered pro-region has no structural effect on p75NTR, and therefore the ability of proNGF to form symmetrical complexes is mainly due to the pro-peptide effect on the mature moiety of the neurotrophin.[6] L2 was already identified as a key difference between these complexes.[3,6]

ProNGF/p75NTR and NGF/p75NTR crystallographic structures present distinct stoichiometries, but it has been observed that both 2:1 and 2:2 stoichiometries may exist in a dynamic equilibrium in solution.[6] Supporting the hypothesis that mature NGF can present the same stoichiometry as proNGF is the 2:2 structure of the mature neurotrophin-3.[6,15] Even though presenting the same stoichiometry, proNGF and mature neurotrophin-3 have different roles in cell survival/apoptosis, suggesting that the 2:2 stoichiometry alone is not sufficient to induce cell death. The ability to have proNGF and mature neurotrophins in complexes with both stoichiometries also suggests that conformational changes might occur with time and spontaneous interconversion between 2:1 and 2:2 stoichiometries occurs. It has been proposed that the asymmetric stoichiometry is an intermediate of the 2:2 complex formation and that the variation between stoichiometries reflects the local concentration of neurotrophins.[6]

In this work, we performed explicit water MD simulations of the proNGF/p75NTR and NGF/p75NTR complexes as well as dimers of the mature and pro-form of NGF to study possible structural rearrangements and their functional consequences. We focused on shedding light in three specific questions: (i) the different stoichiometries referred to in literature; (ii) the importance of the structural rearrangement of the loops with a special focus in L2; and (iii) the role of the receptor binding in the conformational rearrangement of the neurotrophins. The MD simulations of the dimers allowed us to infer the structural and energetic consequences of the NT dimer binding to p75NTR. These simulations showed also that the dimeric structures are not rigid or predetermined solely by the presence or absence of the pro-peptide but can undergo significant structural rearrangements. Here, we portrayed the binding interface between the neurotrophin dimer and its receptor (p75NTR) as well as between the neurotrophin monomers. Indeed, we were able to characterize the effect of the pro-peptide on the NGF structure as well as its effect on receptor binding.

METHODOLOGY

1. Structure Preparation. The proNGF/p75NTR and mature NGF/p75NTR complexes (PDBid 1SG1[3] and 3IJ2[6], respectively) crystallographic structures had missing residues, which were added by homology modeling using the Modeler software[16,17] and the complete amino-acid sequences (GenBank references: P07174 and P01139, respectively). The protonation states of all residues were assigned at physiological range with the PROPKA methodology.[18−21] Mature NGF and proNGF dimers' structures were prepared by eliminating p75NTR chains from the previously obtained complexes.

2. Molecular Dynamic Simulation. The proNGF/p75NTR and the mature NGF/p75NTR complexes were solvated with 25798 and 38988 single point charge waters (SPC),[22] respectively, while NGF and proNGF dimers were solvated with 14954 and 16990 SPC waters, respectively. Then all systems were submitted to 100 steps of steepest descent energy minimization to remove bad contacts between the solvent and the protein. Subsequently, they were equilibrated with a 200 ps molecular dynamics (MD) simulation maintaining the protein atoms restrained by weak harmonic constraints to allow for the structural relaxation of the water molecules. Then, a 100 ns production MD was performed using a time step of 0.002 ps, and the trajectories were saved at each 20 ps. Periodic boundary conditions were used in all simulations. The temperature and pressure were maintained constant by the use of the v-rescale thermostat[23] and Parrinello−Rahman barostat[24] (parameters: τ_T = 0.1 ps, T_{ref} = 300 K, P_{ref} = 1 bar). The Particle Mesh Ewald (PME)[25] method was applied to compute electrostatic interactions with a cutoff of 1.0 nm. A twin range cutoff with neighbor list cutoff 1.0 and cutoff of 1.0 was used for the van der Waals interactions. All the bonds involving hydrogen atoms were kept fixed by the LINCS constraint algorithm.[26] All the simulations were carried out using the Gromacs software package conjugated with the Amber99 force field.[27−30]

3. Structural Analysis. In all the MD simulations, the Root-Mean-Square-Deviation (RMSD) of the protein backbone for the entire complexes as well as for the individual chains was calculated. The plateau was reached upon 10 ns, and therefore the 10−100 ns time frame was chosen to perform the various analyses. For a detailed study of the binding interface, significant residues were selected according to Protein Data Bank in Europe Proteins, Interfaces, Structures and Assemblies tool (PDBePISA).[31] For these residues, B-factors and Root-Mean-Square-Fluctuations (RMSF) were calculated using *ptraj* from the Amber package[32] to investigate their deviation compared to a reference position. To investigate if loops L2 remained in the same position along the MD simulation ("open" or "closed"), the distance between the residues at the

dx.doi.org/10.1021/ci500101n | J. Chem. Inf. Model. XXXX, XXX, XXX−XXX

top of the loop (A Asn46-B Asn46) was measured both for complexes and the dimers. The distance between loops L4 was also measured in the same way (A Lys95 − B Lys95).

4. Energetic Profile. The MM-PBSA (Molecular Mechanics Poisson−Boltzmann Surface Area) script[33] integrated into the AMBER9 package[34] was used to calculate the binding free energy difference upon alanine mutation. The alanine mutations were performed on the interfacial residues that were previously selected in the structural analysis (PDBePISA) with the exception of alanine, glycine, or proline residues. These residues are not mutated either experimentally or *in silico* since they usually have a primary role in the protein stability and their mutation could lead to protein degradation. Due to the limitations of the method, residues that would only interact via backbone could not be analyzed with computational Alanine Scanning Mutagenesis (ASM). This method combines a continuum approach, to model solvent interactions, with a MM-based approach to atomistically model, protein−protein interactions. The MM-PBSA approach first developed by Huo et al.[33] was improved by Moreira et al.[35] and can now be applied with an accuracy of 1.3 kcal/mol.[35] The mutant complexes are generated by a single truncation of the mutated side chain, replacing Cγ with a hydrogen atom and setting the Cβ-H direction to that of the former Cβ-Cγ. For the binding energy calculations, a total of 900 snapshots of the complexes were extracted from 10 to 100 ns of the run. The $\Delta\Delta G$ is defined as the difference between the mutant and wild type complexes as follows:

$$\Delta\Delta G = \Delta G_{\text{cpx-mutant}} - \Delta G_{\text{cpx-wild type}} \quad (1)$$

Typical contributions to the free energy include the internal energy (bond, dihedral, and angle), the electrostatic and the van der Waals interactions, the free energy of polar solvation, the free energy of nonpolar solvation, and the entropic contribution:

$$G_{\text{molecule}} = E_{\text{internal}} + E_{\text{electrostatic}} + E_{\text{vdw}} + G_{\text{polar solvation}} + G_{\text{nonpolar solvation}} - \text{TS} \quad (2)$$

For the calculations of relative free energies between closely related complexes, it is assumed that the total entropic term in eq 2 is negligible as the partial contributions essentially cancel each other.[36] The first three terms of eq 2 were calculated with no cutoff. The $G_{\text{polar solvation}}$ was calculated by solving the Poisson−Boltzmann equation with the software DELPHI.[37,38] In this continuum method, the protein is modeled as a dielectric continuum of low polarizability embedded in a dielectric medium of high polarizability. We used a set of values for the DELPHI parameters that have been shown to constitute a good compromise between accuracy and computational speed.[39] We used a value of 2.5 grids/Å for scale (the reciprocal of the grid spacing); a value of 0.001 kT/e for the convergence criterion; a 90% for the fill of the grid box; and the Coulombic method to set the potentials at the boundaries of the finite-difference grid. The dielectric boundary was taken as the molecular surface defined by a 1.4 Å probe sphere and by spheres centered on each atom with radii taken from the Parse[40] vdW radii parameter set. The key aspect of the new improved approach is the use of a three dielectric constant set of values (ε = 2 for nonpolar residues, ε = 3 for polar residues, and ε = 4 for charged residues plus histidine) to mimic the expected rearrangement upon alanine. This method is described elsewhere.[35,41] It is important to highlight that we used only one trajectory for the computational energy analysis as it has been proven to give the best results.[35] Side-chain reorientation was implicitly included in the formalism by raising the internal dielectric constant. The nonpolar contribution to the solvation free energy due to van der Waals interactions between the solute and the solvent was modeled as a term dependent on the solvent accessible surface area (SASA) of the molecule. This contribution was estimated, using empirical parameters derived from experimental transfer energies of hydrocarbons, as 0.00542 kcal Å^{-1} mol^{-1} SASA + 0.92 kcal mol^{-1}.[33,40] The SASA was determined using the *molsurf* program, which computes the molecular surface defined by Mike Connolly.[42] In this work, we used the standard hot-spot (HS) cutoff: residues that present $\Delta\Delta G_{\text{binding}} < 2.00$ kcal mol^{-1} were considered null-spots (NS), whereas residues with $\Delta\Delta G_{\text{binding}} \geq 2.00$ kcal mol^{-1} were considered HS.

We have also performed alanine shaving, which is the concerted mutation of two or more residues at a time to evaluate their cooperative effect at the protein−protein interface. By calculating the $K_{\text{cooperativity}}$ values described by eq 3 it was possible to compare the effect of replacing two or more residues both separately and together.

$$K_{\text{cooperativity}} = \frac{\Delta\Delta\Delta G}{\sum \Delta\Delta G_{\text{single mutation}}} \cdot \frac{\Delta\Delta G_{\text{multiple mutations}} - \sum \Delta\Delta G_{\text{single mutation}}}{\sum \Delta\Delta G_{\text{single mutation}}} \quad (3)$$

$K_{\text{cooperativity}} = 0$ suggests that the amino-acid residues are functionally independent; $K_{\text{cooperativity}} > 0$ means that a superadditivity effect is verified; $K_{\text{cooperativity}} < 0$ shows that there is a subadditivity effect. Both these effects can be caused by changes in local or global protein conformation, solvent structure, electrostatic fields or dielectric constants, and protein dynamic properties.[43] Subadditivity reflects the fragility of the specific intermolecular interactions, and superadditivity reflects the plasticity and adaptability of the interface.[43] As previously mentioned we have used a set of three different dielectric constants to calculate the $\Delta\Delta G_{\text{binding}}$. When performing alanine shaving, we need to make also concerted mutations of residues belonging to different sets. In this case (i.e., Trp-Glu) we performed our ASM protocol the necessary number of the times with the necessary dielectric constants values and calculated the average value for the $\Delta\Delta G_{\text{binding}}$. For example, for the Trp-Glu mutation we calculated two times the $\Delta\Delta G_{\text{binding}}$ using a dielectric constant of ε = 2 or ε = 4 to determine the average value.

5. SASA Features. SASA, as defined by Lee and Richards,[44] is the area of the surface traced by the center of a probe sphere, whose radius is the nominal radius of the solvent, as it rolls over the van der Waals surface of the molecule. We have determined for the interfacial residues the $_{\text{comp}}\text{SASA}_i$ (the solvent accessible surface area of residue i in complex form) as well as the $_{\text{mon}}\text{SASA}_i$ (the residue SASA in the monomer form). ΔSASA_i, the SASA variation upon complexation, was determined using these features (eq 4).

$$\Delta\text{SASA}_i = |_{\text{comp}}\text{SASA}_i - {}_{\text{mon}}\text{SASA}_i| \quad (4)$$

6. Local Flexibility. The local flexibility along the sequence was calculated along the interval 10−100 ns of each MD

dx.doi.org/10.1021/ci500101n | J. Chem. Inf. Model. XXXX, XXX, XXX−XXX

trajectory. For each residue i, this flexibility parameter was obtained by calculating the fluctuation in the distance d_{ij} between its Cα atom and the Cα atoms of neighboring residues j comprised in the interval (i−2, i+2) along the sequence, weighted by the squared average distance between residue pairs:

$$\text{flex}(i) = \frac{1}{4}\sum_{j=i-2}^{i+2} \langle d_{ij}^2 - \langle d_{ij}\rangle^2\rangle \quad (5)$$

The approach is reminiscent of the local flexibility calculation presented in Morra et al.[45] However, instead of including distance fluctuations for all residues within a given distance range of residue i, here only consecutive residues along the sequence are considered and no distance range is used.

7. Covariance Analysis and Essential Dynamics. The covariance matrix for Cα atoms was calculated along the interval 10−100 ns of each MD trajectory using the *g_covar* analysis tool of GROMACS.[27] The reduced matrix showing the correlation between Cα atoms pairs (i,j) and discussed in the text is derived from the full covariance matrix and is given by $c(i,j)$ entries defined as

$$\begin{aligned} c(i,j) = {} & \langle (x(i) - \langle x(i)\rangle) * (x(j) - \langle x(j)\rangle)\rangle + \langle (y(i) \\ & - \langle y(i)\rangle) * (y(j) - \langle y(j)\rangle)\rangle \\ & + \langle (z(i) - \langle z(i)\rangle) * (z(j) - \langle z(j)\rangle)\rangle \end{aligned} \quad (6)$$

The covariance and reduced matrix, describing the transition between mature and proNGF structure, was obtained using the two crystal structures from NGF/p75NTR (PDBid: 1SG1[3]) and proNGF/p75NTR (PDBid: 3IJ2[6]) complexes. The Essential Dynamics analysis provided by the *g_anaeig* tool of GROMACS[46] was used to determine the Principal Component Analysis (PCA) of the covariance matrix. The MD trajectories were then projected onto the first 4 eigenvectors, accounting on average for 60% of the mobility of the systems, to represent the most significant collective motions. To test the convergence of the MD trajectories, the analysis was repeated on two separate trajectory halves, by considering two time intervals: 5−50 ns and 50−100 ns.

8. Root-Mean-Square-Inner-Product (RMSIP). RMSIP[47,48] was used to compute the similarity between two sets of eigenvectors obtained from the PCA analysis

$$\text{RMSIP} = \sqrt{\frac{1}{N}\sum_{i=1}^{m}\sum_{j=1}^{m}(v_i \times w_j)^2} \quad (7)$$

with v_i and w_j as the ith and jth eigenvectors of the two sets. We split each of the four MD simulations in two separate trajectory bits, corresponding to time intervals 5−50 ns and 50−100 ns and calculated the similarity between the essential eigenspaces of the two halves.

RESULTS

1. Structural Analysis. RMSD profiles were calculated, for the complexes (NGF/p75NTR and proNGF/p75NTR) as well as for the individual chains (Figure S1; Supporting Information), to analyze their stability. These plots also allowed us to understand the motion and stability of each chain and analyze their dynamical behavior. Figure S1A shows that the NGF chains in the NGF/p75NTR complex present lower deviations along the MD simulation, when compared to the p75NTR chain. We can also point out that NGF chain A shows a lower RMSD value (<RMSD> = 1.73 Å ± 0.26 Å) than the NGF chain B (<RMSD> = 2.01 ± 0.21 Å). However, chain B shows lower fluctuation along the simulation and therefore is more stable. In the proNGF/p75NTR complex (Figure S1B), the NGF chain A also presents greater stability than the p75NTR chain Y (lower RMSD values and lower fluctuation; <RMSD> = 2.63 ± 0.41 Å). Nevertheless, p75NTR chain X presents (<RMSD> = 1.68 Å ± 0.25 Å) similar stability to the NGF chains. In both complexes the RMSD of the whole complex is strongly influenced by the stability of the p75NTR chains, which present greater instability closer to the L3 loop of the NGF chains.

In order to infer if the stability of the NGF and proNGF dimers results from complex formation with the receptor p75NTR, RMSD profiles were also obtained for the uncomplexed neurotrophin dimers in solution (Figures S2 and S3). The structure of the dimers presents greater deviation from the initial structure than the one observed in their complexes with p75NTR. For the mature NGF dimer (Figure S2A) both NGF chains present similar maximum values of RMSD. However, NGF chain B presents greater fluctuation than chain A (Figure S2A). These results show that p75NTR binding to the mature NGF dimer increases the stability of the chains and changes the dynamic properties of the NGF dimer, reducing the fluctuations of NGF chain B along the simulation. In the proNGF dimer (Figure S2B), it was also possible to observe an increase of the RMSD values for both chains. However, unlike the mature NGF dimer, no noticeable differences were detected for the dynamic behavior of these chains when compared to the complex with p75NTR. Both NGF chains present similar maximum RMSD values and stability profile. Nevertheless, we have to highlight that between 40 and 60 ns, it was observed a significant increase in RMSD values. Figure S3B demonstrates that this deviation comes from reorientation of the loops portion of the dimer. On the remaining biological systems the RMSD of both loops and structured areas has a more similar behavior.

2. Structural and Energetic Profiling. We performed computational ASM to characterize the molecular interfaces of the mature NGF/p75NTR and proNGF/p75NTR complexes as it allows the depiction of the key interactions at these interfaces. Tables S1 and S2 (Supporting Information) list the decomposition of the free binding energy into its additive contributions, adequately representing the systems with the sum of its contributions. For both complexes two interfaces were analyzed: NGF/p75NTR and NGF/NGF in which we found specific residues that seem to have an important role − HS (Figures 2 and 3). A direct comparison between the computational and experimental ASM was performed for all cases with available experimental data (Tables S1).

2.1. Mature NGF/p75NTR. Six HS only involved in p75NTR binding were identified in this interface, while the other six were identified as relevant for NGF/p75NTR as well as for the NGF/NGF interfaces. Although previous works with the mature NGF/p75NTR complex did not refer to a third site (His75 was considered part of Site 2) by computational ASM technique, we identified the HS in three binding sites, which is in accordance with previous findings with the mature neurotrophin-3 and proNGF.[6,15]

Figure 2 show that p75NTR is not equally inserted in the NGF dimer. Binding Site 1 is better inserted in the binding crevice than binding Sites 2 and 3 and therefore possesses a

dx.doi.org/10.1021/ci500101n | J. Chem. Inf. Model. XXXX, XXX, XXX−XXX

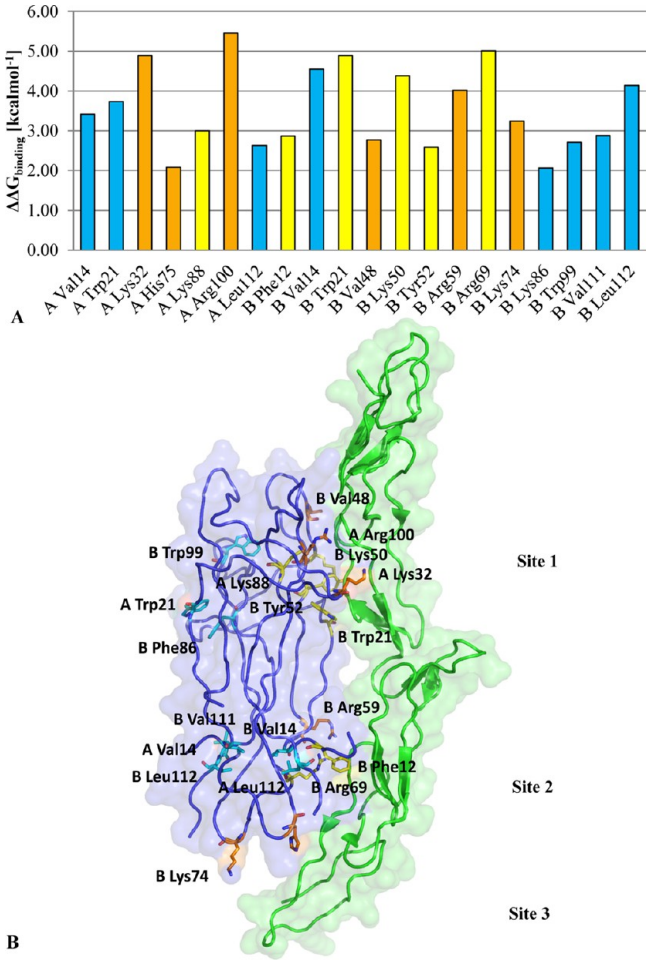

Figure 2. Graphical representation of the relative free binding energy of the detected HS in (A) mature NGF/p75NTR complex and its structural representations (B). HS are in stick representation and highlighted in orange for residues in the mature NGF/p75NTR interface, blue for residues in the NGF/NGF interface, and in yellow are represented residues common in both interfaces. NGF chains are highlighted in blue and p75NTR chains in green.

higher number of HS (seven HS in comparison to three HS for binding Site 2 and two HS for binding Site 3). HS involved only at the p75NTR interface are A Lys32, A His7, A Arg100, B Val48, B Arg59, and B Lys74. Several HS in common between this interface and the NGF/NGF interface were identified: A Lys88, B Phe12, B Trp21, B Lys50, B Tyr52, and B Arg69.

The majority of the HS can be classified in two types: charged and aromatic residues. With this analysis we verified the hypothesis that the residues responsible for p75NTR binding would be the positively charged residues from NGF.[3] Table S3 lists all the H-bonds and salt-bridges involving the HS at this system. The vast majority of the H-bonds are formed between residues only important for the NGF-NGF interface (B Trp99 and A Trp21). The salt-bridges involve residues important for the dimeric form as well as the complex binding. A Lys 32, A Arg100, B Arg59, B Arg69, and B Lys74 are some of the residues with a higher number of these contacts, which justifies their main role as HS. Lys74 and His75 were computationally identified in Site 3. Lys74 cannot be directly detected as an important residue for binding solely by X-ray structure inspection (PDBid: 1SG1[3]) as in this static image this residue appears to be distant from p75NTR for any ionic interactions to take place. During the MD simulation, the structure of NGF remains very stable, but movement of p75NTR near sites 2 and 3 can be observed. This movement is not observed near Site 1, and the reason might be the distance into the binding crevice of the NGF homodimer. In Site 1, p75NTR is located closer to the NGF molecules than in Site 2, which in its turn is closer than Site 3. This is also in agreement with the number of HS detected that decreases along the binding sites.

2.1.1. Mature NGF/NGF Interface. The major contributing determinants for the NGF/NGF interface depicted in Figure 3 are A Val14, A Phe54, B Arg69, B Phe86, B Lys88, B Val 111, B Leu112, and B Arg114. All these HS are residues with hydrophobic side chains and their main contribution is through $\Delta\Delta E_{VDW}$ due to their capability to stack aromatic side chains. As referenced in the NGF/p75NTR interface several HS are common to both interfaces, and these are A Lys88, B Phe12, B Trp21, B Lys50, B Tyr52, and B Arg69. From these results, it is possible to infer that the most relevant types of contributions for binding of the NGF dimer are not only the van der Waals forces but as well the formation of H-bonds and salt-bridges. Residues with great contribution for relative free binding energy of the NGF dimer also appear localized in four distinct sites: two belonging to Sites 1 and 2 for the NGF/p75NTR and another two located on their opposite direction.

Different authors performed alanine shaving of some residues at the mature NGF/p75NTR system.[41,49] We have also performed the concerted mutation of crucial residues at this interface (Table S4) and calculated the $K_{cooperativity}$. The use of this parameter relates to the possibility of error cancelation and therefore a better comparison between the sum of the $\Delta\Delta G$ of individual mutations and the $\Delta\Delta G$ of multiple mutations. It is especially important the introduction of this parameter to analyze our results of the alanine shaving procedure as multiple mutations have in principle higher conformational changes, which may be not correctly characterized by our one trajectory methodology. Tables S1 and S4 show that we were able to correctly calculate (within the theoretical error of 1.3 kcal/mol),[35,41] the $\Delta\Delta G_{binding}$ for 7 out of the 10 mutants. Although they are in reduced number, it is possible to perceive that our reliable computational alanine scanning technique[35,41,50] works well in this system. However, some deviations from the experimental values can be encountered due to inherent inaccuracies of the force field, lack of explicit atomic polarization, incomplete exploration of the side-chain conformational space, and even the use of a single trajectory protocol. The last sources of uncertainty have been implicitly corrected in an average way through the consideration of different dielectric constants for different amino acid residues, which constitutes the conceptual backbone on the methodology. Nevertheless, in some situations the microenvironment around each amino acid varies substantially and cannot be perfectly corrected through an empirical parameter calibrated to reflect the most common scenarios.[35,41,50]

Table S4 shows that for the majority of the multiple mutants there is not an additivity effect. Contrarily, they are shown to have a subadditivity or superadditivity effect. We have to stress out the triple mutant Lys74ALA/His75ALA/Asn77Ala, which was shown not to bind to the p75NTR monomer with a $\Delta\Delta G_{experimental}$ higher than 1.65 kcal/mol, and for which we have attained a $K_{cooperativity}$ value of 2.37.[41,49] Concerted mutation of Asp72Ala/Ser73Ala/Lys74Ala was experimentally demonstrated to have a compensatory effect ($\Delta\Delta G$ of 0.12

dx.doi.org/10.1021/ci500101n | J. Chem. Inf. Model. XXXX, XXX, XXX−XXX

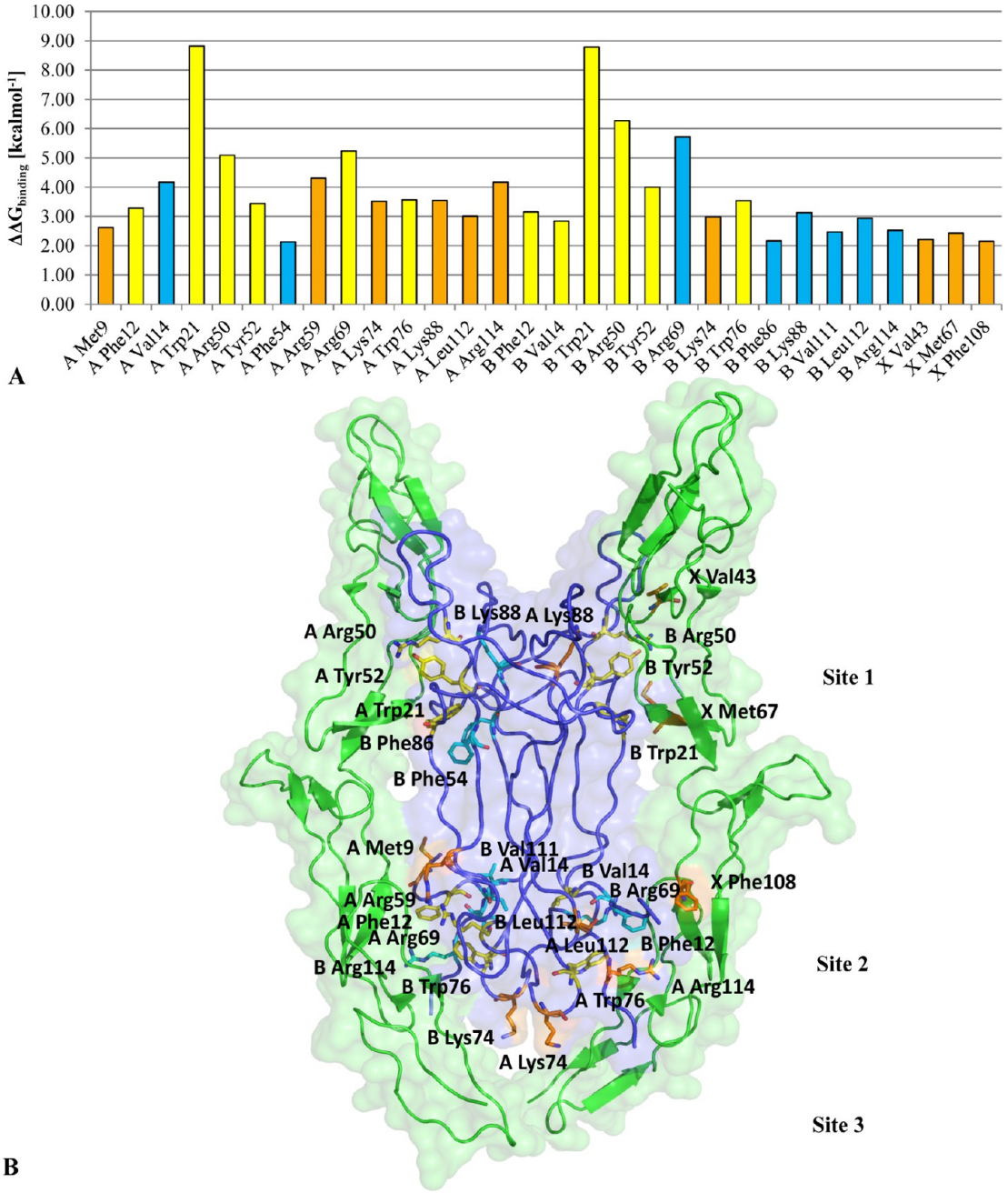

Figure 3. Graphical representation of the relative free binding energy of the detected HS in (A) the proNGF/p75NTR complex and its structural representations (B). HS are in stick representation and highlighted in orange for residues in the proNGF/p75NTR interface, blue for residues in the proNGF/NGF interface, and in yellow for the common residues to both interfaces. ProNGF chains are highlighted in blue and p75NTR chains in green.

kcal/mol) such that the binding of the mutant p75NTR is comparable to the wild type NGF.[41,49] This mutant shows a $K_{\text{cooperativity}}$ value of 1.14 but a $\Delta\Delta G_{\text{multiple mutations}}$ of only 1.07 kcal/mol.

2.2. ProNGF/p75NTR. For the proNGF/p75NTR complex, we identified three binding sites as illustrated in Figure 3B. In the interface of this complex, we detected residues exclusively involved in its stabilization and others that also contribute for proNGF/proNGF binding. The HS that exclusively contribute to p75NTR binding are A Met9, A Arg59, A Lys74, A Lys88, A Leu112, A Arg114, and B Lys74 and from the p75NTR chain X: X Val43, X Met67, and X Phe108. Residues identified as HS for both interfaces are A Phe12, A Trp21, A Arg50, A Tyr52, A Arg69, A Trp76, B Phe12, B Val14, B Trp21, B Arg50, B Tyr52, and B Trp76. As in the complex with mature NGF, the greater contributions for relative free binding energy are $\Delta\Delta E_{\text{Ele}}$ from charged residues and $\Delta\Delta E_{\text{VDW}}$ for residues with hydrophobic side chains. Although Trp76 from NGF's chain A and B are HS located near Lys74 (loop L3) their interaction with p75NTR molecules seems to be preferentially with residues in Site 2 due to the position of their side chain. Having this fact in mind we included it in the binding Site 2. It is to notice that there are some important differences between the interfaces with the different p75NTR molecules (chains X and Y) as the number of significant residues for binding of p75NTR chain X is higher than for chain Y (13 versus 10 HS). Besides residues at chain X

dx.doi.org/10.1021/ci500101n | J. Chem. Inf. Model. XXXX, XXX, XXX−XXX

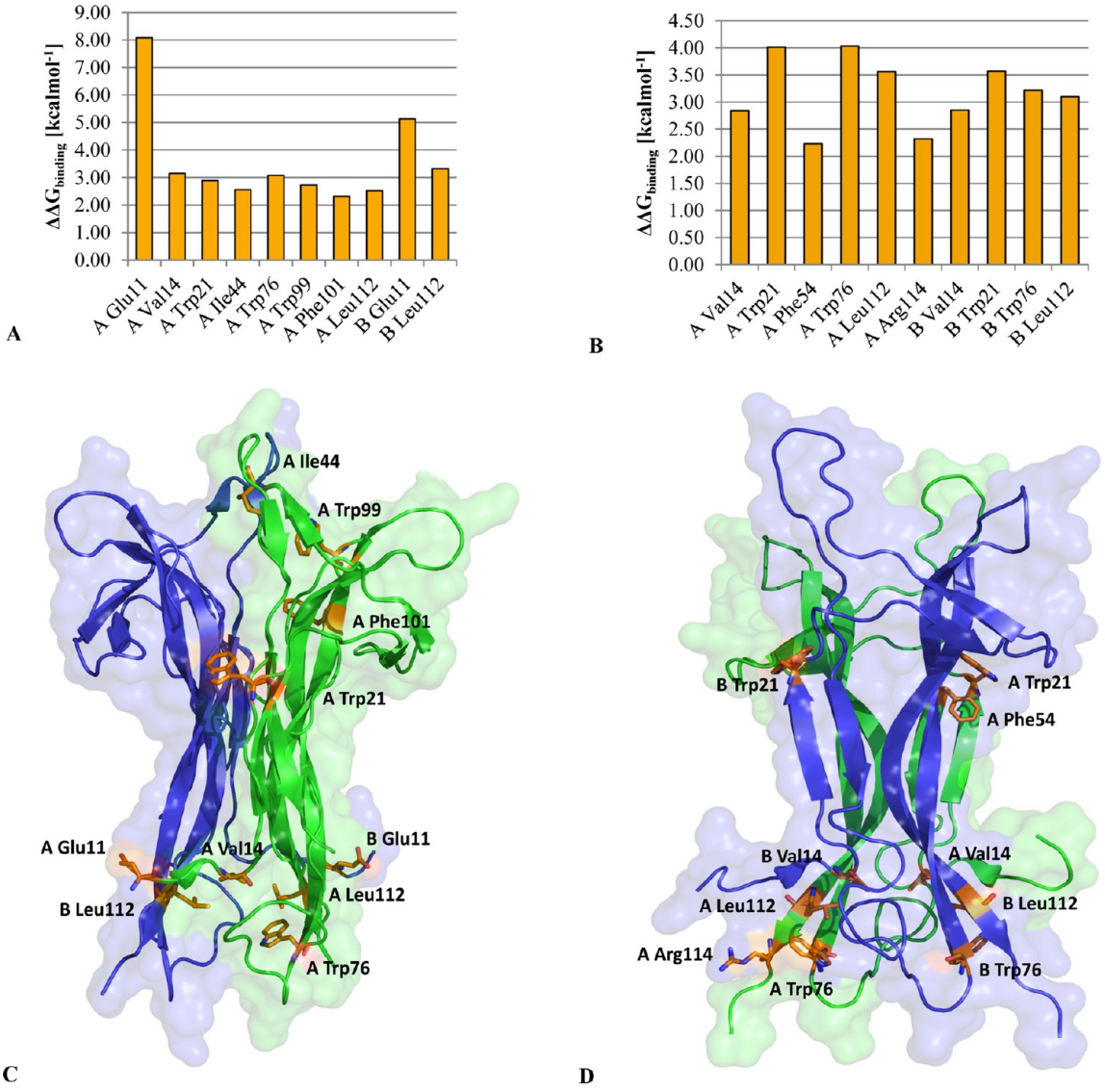

Figure 4. Graphical representation of the relative free binding energy of the detected HS in the NGF (A) and proNGF (B) dimers. Bottom panels illustrate the structural representations of NGF (C) and proNGF (D) dimers. HS are in stick representation and highlighted in orange. Chains B are highlighted in blue and chains A in green.

are much more involved in the formation of crucial H-bonds and salt-bridges with HS at the NGF dimer than residues at chain Y (Table S5). Another important aspect is the fact that only chain X presents relevant residues for p75NTR binding as inferred with the ASM methodology (zero HS in chain Y). This is reflected in the increased dynamics of chain Y relative to NGF and particularly in the asymmetric motion of the C terminal subdomain of chain Y. Notably, this result is in agreement with the experimental B factors staying locally higher in this region. These aspects might be indicative of one of the p75NTR molecules having weaker binding to the NGF dimer, which could evince that one (chain Y) is more prone to be released from the complex leading to a 2:1 stoichiometry. These results strength the hypothesis of Feng et al.,[6] that the complex exist in *equilibrium* with 2:2 and are further supported by the results from the structural analysis previously presented.

2.2.1. ProNGF/proNGF Interface. As referenced in proNGF/p75NTR interface there are HS involved in both interfaces which are A Phe12, A Trp21, A Arg50, A Tyr52, A Arg69, A Trp76, B Phe12, B Val14, B Trp21, B Arg50, B Tyr52, and B Trp76. As in NGF/p75NTR complex, the majority of the residues involved in NGF/NGF binding are residues with hydrophobic side chains capable of establishing van der Waals interactions. However, unlike the complete complex of proNGF/p75NTR, the majority of the contribution for relative free binding energy with charged residues is the result of positively charged residues from the proNGF domain instead of a balanced contribution between positively and negatively charged residues.

In the proNGF structures there are a higher number of H-bonds and salt-bridges compared to the mature one (Table S5), which is related to the presence of the second p75NTR monomer. These interactions involved mainly B Arg 69 (occupancy around 100%), A Lys88 (around 95% of occupancy), and A Arg50 (ranging from 30 to 69%). In this complex the majority of the multiple mutations (Table S6) seem to be subaddivity and blocking the effect of single mutations as the one involving B Phe12/B Val 14 with a $K_{cooperativity}$ of −1.97.

dx.doi.org/10.1021/ci500101n | *J. Chem. Inf. Model.* XXXX, XXX, XXX−XXX

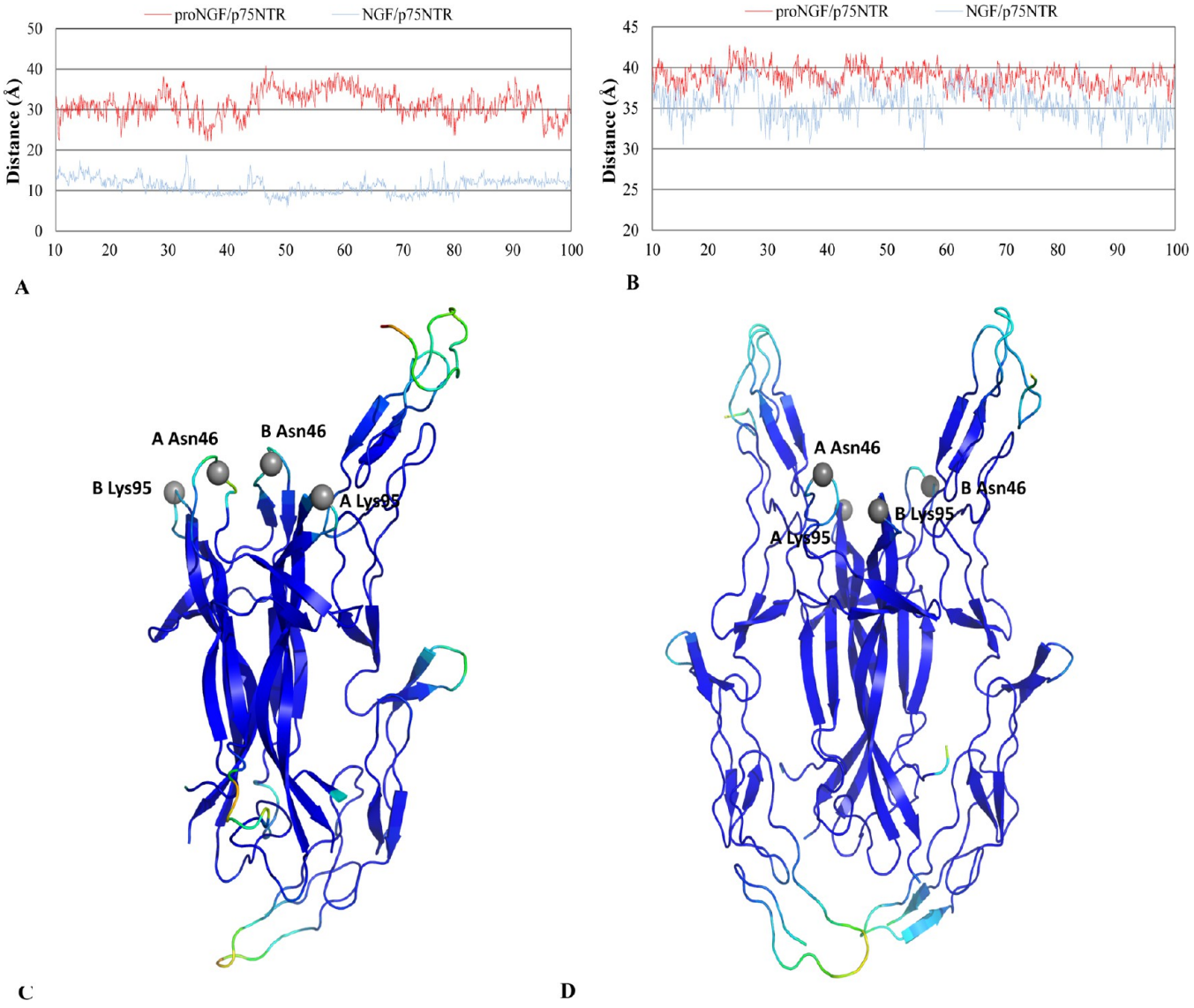

Figure 5. Graphical representation of the distance between L2 (A) and L4 (B) loops for the complexes proNGF/p75NTR and NGF/p75NTR. In the bottom panels are the graphical representations of the B-factor using color scale in the NGF/p75NTR (C) and proNGF/p75NTR (D) complexes. Residues used to measure the loop distances are in a spherical representation.

2.3. NGF and proNGF Dimers MD Simulations. In order to better comprehend the influence of p75NTR binding in the mobility and energetic characteristics of the NGF dimers, ASM was also performed for the residues on the interfaces in Figure 4. The results are presented in Tables S7 and S8. H-bonds and salt-bridges are only presented for mature NGF (only 4 with occupancy higher than 30%) as in the proNGF interface we have not detected any (Table S9). With this analysis, we observed that the presence of HS between the chains in the proNGF dimer appears more equally divided between the two chains than in the NGF dimer, and with most HS being the same residues within each NGF chain. In the mature NGF dimer most of the HS were identified in chain A which was shown to be the most stable one of this dimer. This behavior is opposite to the one found upon p75NTR binding, where most HS were identified in the NGF chain B. Therefore, it is likely that binding of the p75NTR molecule stabilizes chain B while destabilizing chain A. This might be one of the reasons why mature NGF in complex with p75NTR presents a 2:1 stoichiometry in the crystal structure. An important difference was the identification of Glu11 as a HS for both chains in the mature NGF case. In the proNGF dimer, these residues do not have a great impact in binding of the neurotrophin moiety. The presence of additional residues at the N-terminal does not allow a tightly pack of the two opposite proNGF chains. As shown in Figure S4, the HS involved in the NGF/NGF binding in the absence or presence of p75NTR are clearly different. In the mature NGF:p75NTR complex, only residues A Lys 14, A Trp21, and B Leu112 act as HS. The low number of HS can be explained by the position of these residues in relation to the p75NTR binding sites. Being in the opposite side from the receptor binding site, these residues do not suffer the same structural modifications as in the monomer in direct contact with p75NTR. These allow a more permanent stability of the residues leading to a more constant positive effect in NGF/NGF binding. As seen in Figure 4A, the NGF residues, which are also involved in p75NTR binding in the mature NGF/p75NTR, do not act as HS for the dimer formation. This data show that binding to the p75NTR produces structural rearrangement in the neurotrophin dimer that not only affects

dx.doi.org/10.1021/ci500101n | J. Chem. Inf. Model. XXXX, XXX, XXX−XXX

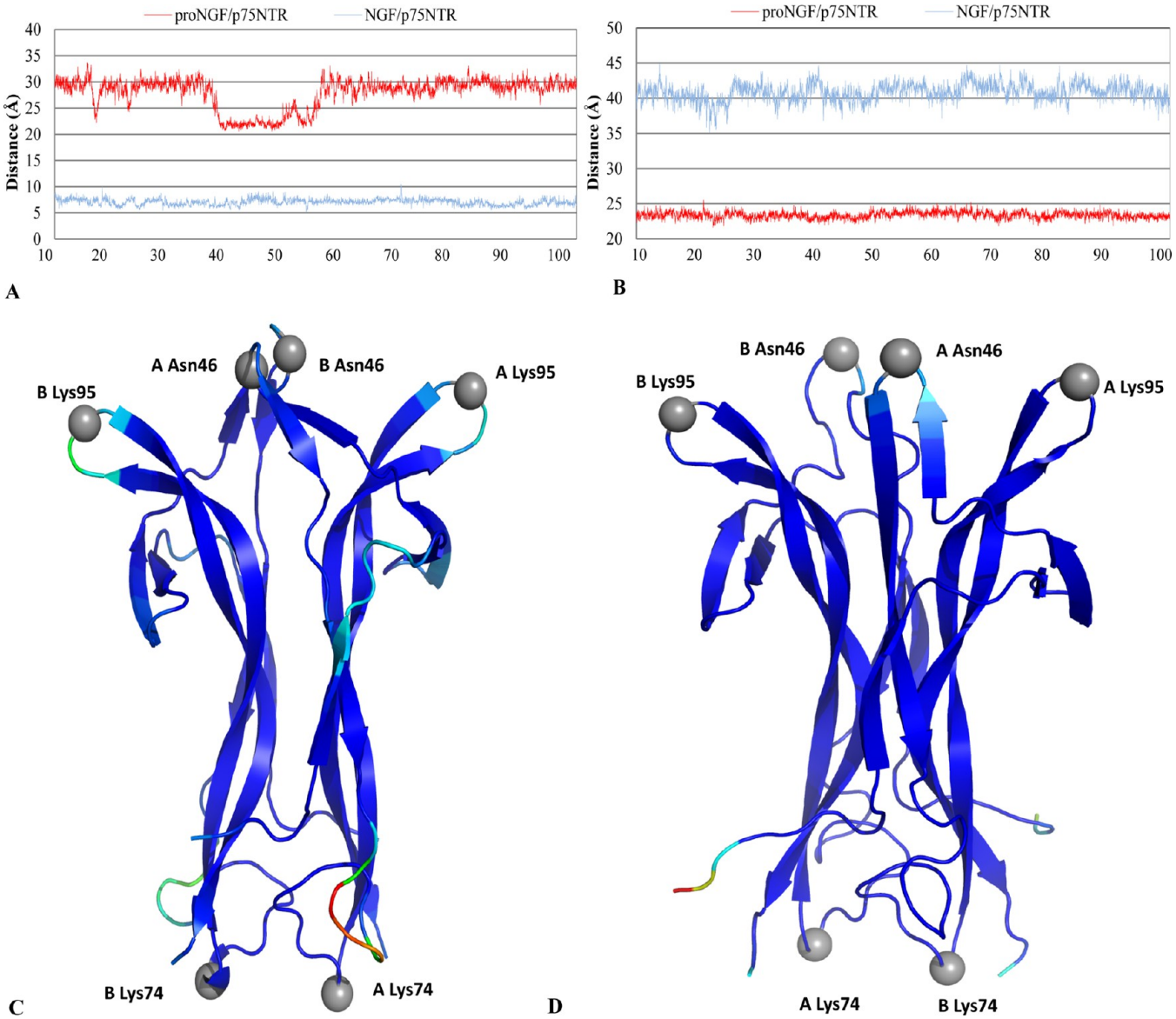

Figure 6. Graphical representation of the distance between L2 (A) and L4 (B) loops for complexes proNGF and NGF dimers. In the bottom panels are represented the NGF structure colored by B-factor in the mature dimer (C) and proNGF dimer (D) complexes. The residues used to measure the loop distances are in a spherical representation.

structure and dynamics but as well the HS involved in the NGF/NGF dimer. The structural modifications, which are distances between loops and position of the residues on NGF/NGF upon p75NTR binding, do not have only a positive effect in NGF/NGF binding. Residues A/B Glu11, A Ile44, A Trp76, A Trp99, and A Phe101 were also detected as residues determinants for binding in the dimer. However, upon complexation to the receptor, these residues show an inferior relative free binding energy or are even not present in the NGF/NGF interface stressing out the effect of p75NTR on the neurotrophin dimer.

The complexes formed with proNGF show similar behavior as the ones formed with mature NGF with residues Arg50, Tyr52, and Arg69 from both chains shown to be relevant for the dimer stability only upon p75NTR binding. The stabilization of the NGF chains by these residues is highly ruled by the lower distance to the binding sites on the complex with p75NTR that leads to stronger interactions. Trp21 and Val14 in both proNGF chains are detected as HS for both complexes, unlike what was verified for the mature NGF. This is in accordance with the previous discussion and demonstration of the existence of a greater stability and symmetry of the neurotrophin chains within proNGF than within the mature NGF.

Table S10 shows the results for the multiple mutations at these interfaces. The results are very different from the ones attained for all the complexes specially when comparing with the mature NGF/p75. Most of the mutations are subadditive, and therefore specific pair interactions do not seem to have the same degree of importance as for the complexes.

SASA features have been proven useful in HS detection,[51] and in this work we have estimated ΔSASA for all interfacial residues in all the analyzed interfaces. Average ΔSASAs for HS and NS residues are represented in Figure S5. This figure illustrates that the average ΔSASA is higher for HS than for NS and therefore shows that residues identified as HS present greater difference of SASA upon complex formation. These results are in agreement with previous works on the occlusion

dx.doi.org/10.1021/ci500101n | J. Chem. Inf. Model. XXXX, XXX, XXX−XXX

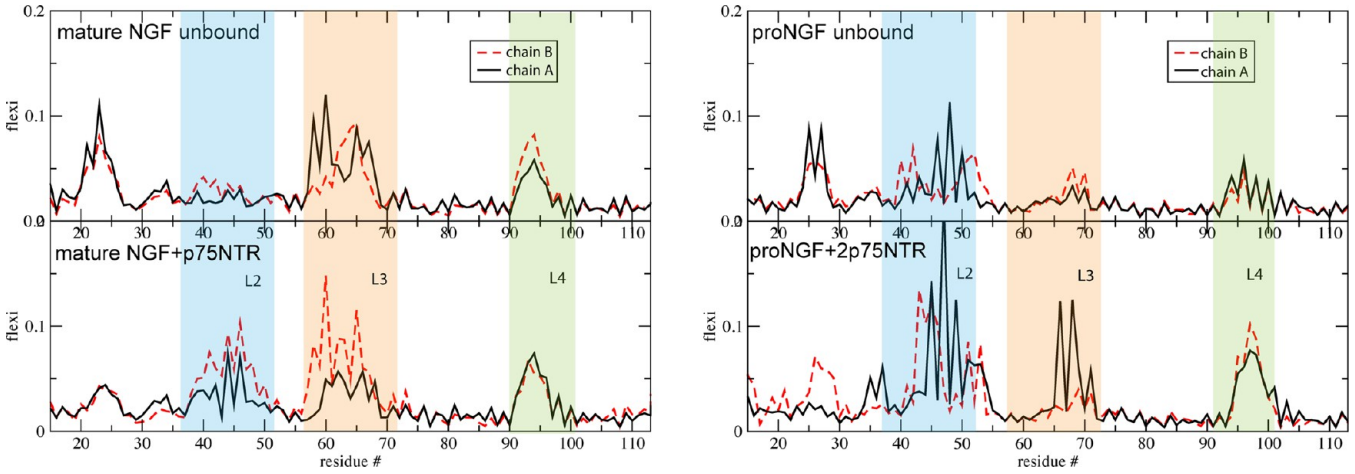

Figure 7. Local flexibility profile of the two NGF monomers under different conditions. Left, mature NGF in the unbound state (top) and complexed with one p75NTR chain (bottom). On the right, proNGF is presented in the unbound state (top) and in the bound state with the two p75NTR chains (bottom). Loops L2, L3, and L4 are highlighted in blue, orange, and green, respectively.

from the solvent as an important determinant for the HS character of an interfacial residue.[50,51] The difference in average ΔSASA between HS and NS is very similar between similar complexes even though the neurotrophin chains are different. To better characterize the interfacial residues behavior, we have calculated the RMSF (Figures S6 and S7), and this factor demonstrates that on average the HS have lower fluctuations than the computationally detected NS. This behavior was already demonstrated in previous studies.[52]

3. Loops Dynamics. One of the key differences between mature NGF and proNGF in complex with p75NTR is the position of the L2 loops from the NGF moiety. To infer if the "open" and "closed" state of the L2 loops is retained (in the proNGF/p75NTR and NGF/p75NTR complexes, respectively) the distance between two anchor positions of the loop of each NGF molecule was calculated (Figure 5). As shown in this figure there is a significant difference between the distances of the L2 loops for both complexes. This clearly shows that both "open" and "closed" states are maintained during the MD simulation for the proNGF (average value of 31.38 Å) and mature NGF (average value of 11.15 Å), respectively. We have also observed structural rearrangements of the L4 loop along the MD simulation (Figure 5B). Loops L4 are clearly oriented in a different manner, in close proximity to the center of the NGF dimer in the NGF/p75NTR. This difference might also be a structural effect of the pro-peptide on the NGF moiety. Figure 5C and D shows that, in both complexes, the loops within the NGF homodimer are the secondary structural motif with greater variance in the NGF molecule with the remaining system very stable. P75NTR in the NGF/p75NTR complex (Figure 5C) presents greater variability at the extremities of the receptor, which might be the result of the lower number of interactions established with the NGF moiety and the lower number of disulfide bonds. As in NGF/p75NTR, the p75NTR chains within the proNGF/p75NTR complex have greater variability at the extremities of the chain. It is important to notice that the "bottom" of the p75NTR chain Y has greater variance than the same portion in its homologue p75NTR chain X, which is in accordance with the RMSD analysis (Figure S1).

Given the importance of the "open"/"closed" states for this neurotrophin activity, distances between loops L2 and L4 were also measured for the NGF dimers in solution that allowed evaluating if these states remain in the absence of the receptor (Figure 6). We observed the maintenance of their states. However, as already observed in the RMSD profiles, there is a significant difference at the interval 40−60 ns for the proNGF. An approximation of loops L2 is observed suggesting an intermediate state for the pro-form of NGF. A significant decrease between loops L4 is also encountered for the dimer in comparison with the dimer/receptor complex. The lack of the p75NTR chains allows the relocation of L4. In the mature NGF dimer, no difference is encountered. This is due to the "closed" state of loops L2, which prevents the approximation of loops L4 in order to avoid steric clashes. Figure S8 illustrates in another comparative way the differences between the distances of L2 and L4 on the four MD simulations.

3.1. Loops Dynamics 2- Local Flexibility. The local flexibility along the protein chains (see Methods) was calculated in the four different systems (bound-unbound state for proNGF and mature NGF). The aim was to evaluate the modulation of the loops dynamics in the proNGF and NGF structures as resulting from the different structures as well as from binding to the receptor. In the absence of the receptor, the profile of local flexibility of both NGF monomers indicates a different behavior of the loop regions in pro- and of the mature structure. This is associated with a modulated mobility at the regions of the binding Site 1 as well as L2, L3, and L4. In particular, the mature NGF (Figure 7, left, top) has mainly localized mobility at the exposed L3, whereas L2 are rigid as a probable effect of their mutual interaction. Otherwise, the L4 loop is relatively flexible. In contrast, the proNGF (Figure 7 right, top) shows no significant motion of loop L3. However, the L2 loop is here more exposed of L2 and is followed by the decrease of mobility of L4. In the presence of the receptor (Figure 7 left and right, lower plot), both pro- and mature species undergo a flexibility modulation, mainly involving loops L2 and L3. In both constructs, the loops increase their motion in the presence of the receptor. Due to the enhanced motion of loops L2 in the mature NGF and of L3 in the proNGF, the flexibility profiles of p75NTR-bound proNGF and mature NGF monomers become more similar to each other than they are in the absence of the receptor. This is observed in the mature construct for the NGF moiety contacting p75NTR at loop L2.

dx.doi.org/10.1021/ci500101n | J. Chem. Inf. Model. XXXX, XXX, XXX−XXX

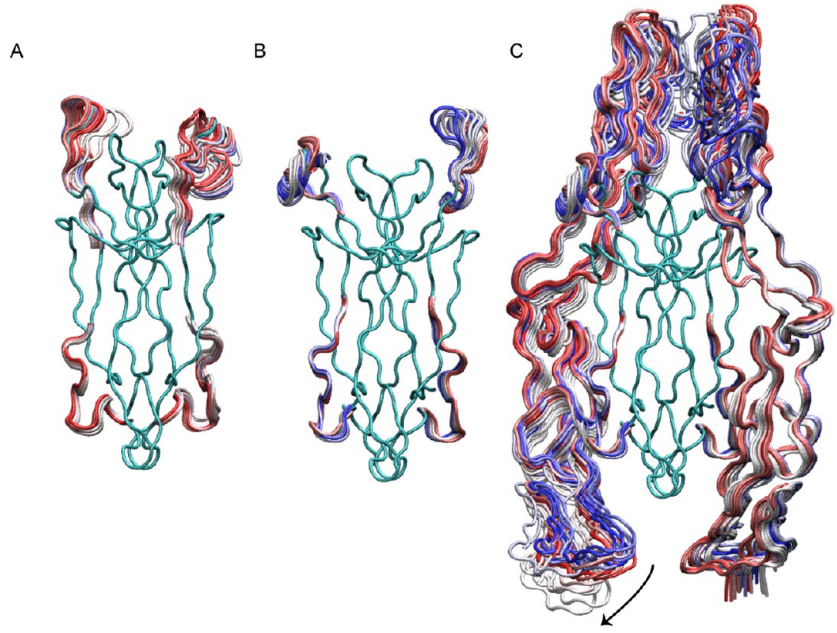

Figure 8. Essential Dynamics analysis of the proNGF system. The bundle of 20 snapshots, colored from red to blue according to the time step, covers the whole MD trajectory and results from its projection onto the first 4 essential eigenvectors. Only L2, L3, and p75NTR are explicitly shown. A) unbound proNGF, B) C) proNGF bound to p75NTR, showing the projection of NGF loops L2 and L3 (B) and the projection of chains p75NTR (C). The arrow in (C) indicates the motion of the second p75NTR chain.

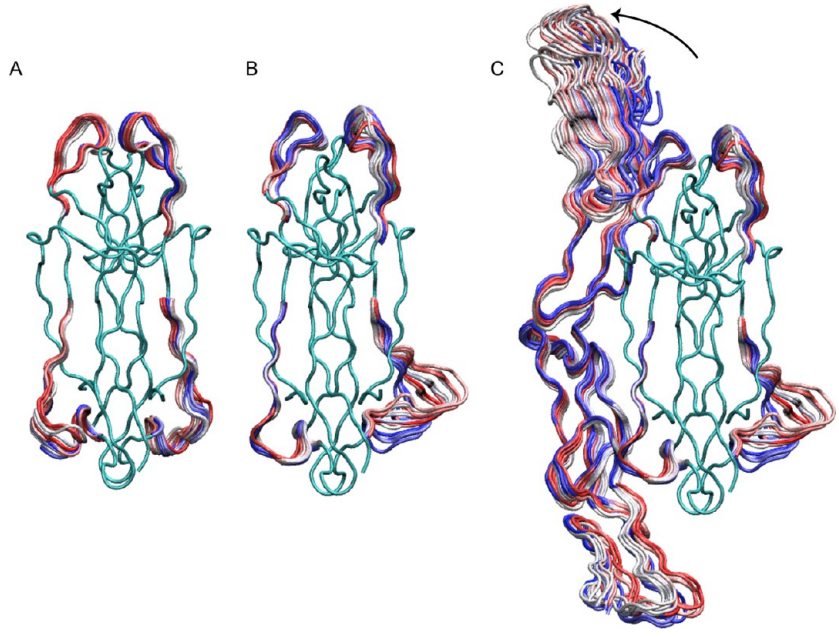

Figure 9. Essential Dynamics analysis of the mature NGF system. The bundle of 20 snapshots, colored from red to blue according to the time step, covers the whole MD trajectory and results from its projection onto the first 4 essential eigenvectors. Only L2, L3, and p75NTR are explicitly shown. A) unbound mature NGF. B) C) mature NGF bound to p75NTR, showing the projection of NGF loops L2 and L3 (B) and the projection of chain p75NTR (C). The arrow in (C) indicates the motion of the p75NTR chain.

Here, the increase in mobility is compensated by the enhanced rigidity of the N-terminal region of binding Site 1 residues 20–25, of both chain A and chain B. Interestingly in the proNGF (right), the same N-terminal region binding Site 1 appears more rigid in chain A, whereas chain B does not show a significant modulation with respect to the unbound case. This again suggests that the binding of p75NTR to chain B might be less tight than it is to chain A, as indicated by the RMSD and computational ASM analysis. Overall, these findings provide evidence that loops L2 and L3 strongly respond to the receptor, by inducing a dynamically activated state in both NGF systems. In particular, the enhanced flexibility of loop L2 in the mature NGF monomer might facilitate the interconversion between the "closed" and "open" conformation of the loop.

The profile of the p75NTR molecule (Figure S8) is on the other hand rather constant in both systems and is characterized by a significantly low local flexibility, which can be explained by the presence of many disulfide bridges all along the receptor

dx.doi.org/10.1021/ci500101n | J. Chem. Inf. Model. XXXX, XXX, XXX–XXX

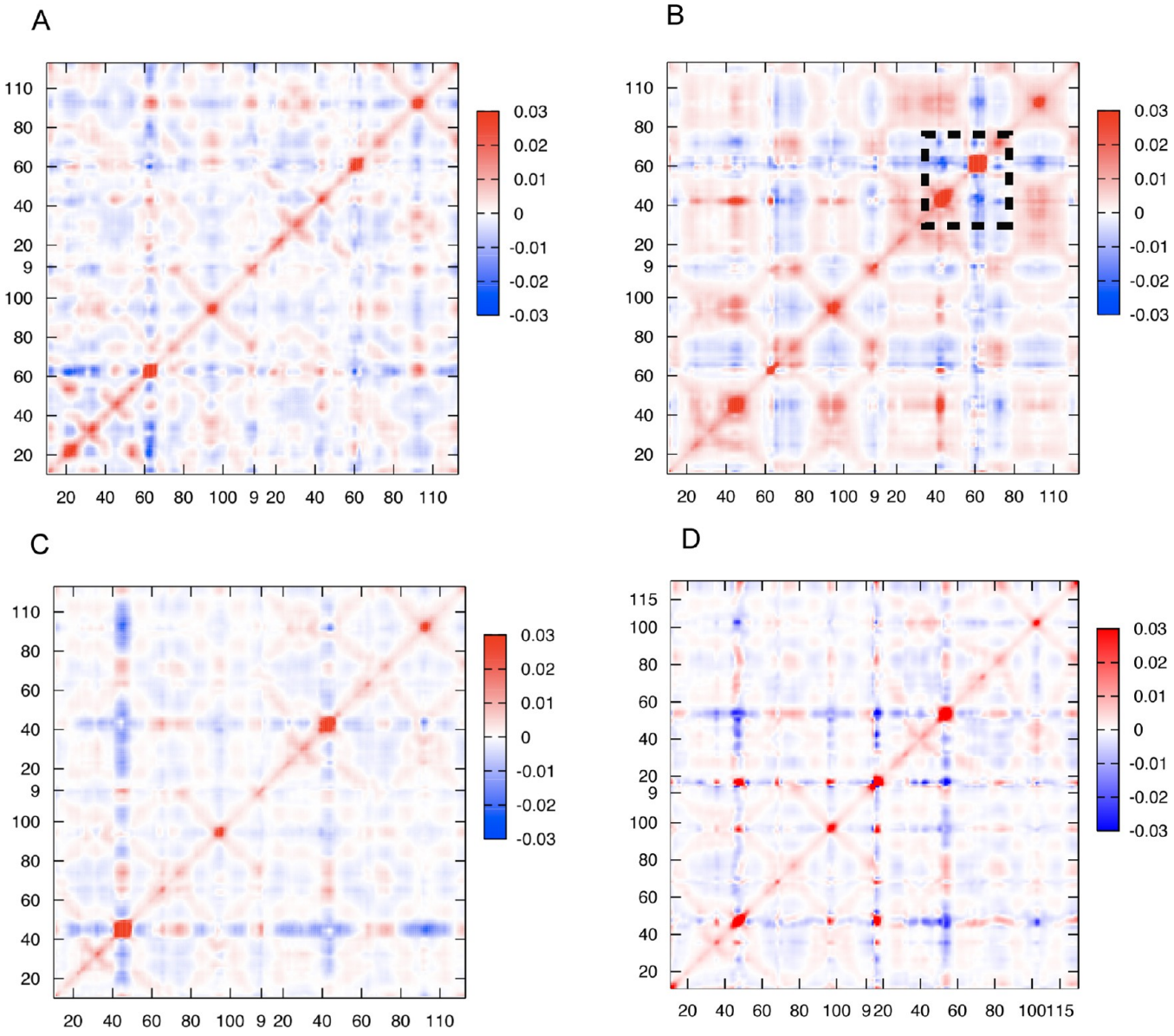

Figure 10. Reduced covariance coefficients of the NGF dimer A) mature NGF in the unbound state; B) mature NGF bound to one p75NTR chain; C) proNGF in the unbound state; and D) proNGF bound to two p75NTR chains. The dashed box in B highlights residues 40−70 of the second monomer, including loops L2 and L3.

structure. Interestingly, a remarkable increase of flexibility is present at residues 150−160 toward the C terminal end of the second chain. Overall, the asymmetric presence of high B-factors values at the C-terminal subdomain on the second p75NTR chain in the proNGF complex (see previous section) and the rather uniformly low local flexibility, resulting from this analysis, are compatible with a very localized rigid-body motion of the second p75NTR subdomain more pronounced than in the other p75NTR chain. This dynamic asymmetry points to a lower stability of the interface with the second p75NTR chain.

3.2. Essential Dynamics Analysis. 3.2.1. Dynamics of the p75NTR Chains. The Essential Dynamics analysis provides information on the relevant collective motions characterizing the complexes. In order to describe the interactions between p75NTR and NGF, we analyzed the motion of the receptor chains with respect to the pro- and mature NGF in both 2:1 and the 2:2 complexes. In the latter, given the increased RMSD of the second p75NTR chain together with the modulation of local flexibility only on one side of the NGF moiety, we expected an asymmetric motion of the two p75NTR chains. Indeed, the projection of the MD trajectory on the first four essential eigenvectors (accounting for the 60% of the covariance; Figure 8C) provides evidence that the second p75NTR chain undergoes a significant collective motion. This results in a displacement away from its proNGF partner, relative to the starting conformation. The motion is particularly enhanced at the C-terminal side of p75NTR, in agreement with the experimental B-factors, and affects the distance of receptor to the L3 binding site on chain A. The other p75NTR (chain X) does not show this behavior, and both C- and N- terminal contact regions remain close to the initial structure. Overall, these findings support the hypothesis that the second p75NTR chain is less tightly bound to the proNGF on the L3 binding site than the first one is. Therefore, it undergoes significant deviations from the initial complex. This also explains the increased local flexibility observed for L3 in proNGF chain A.

dx.doi.org/10.1021/ci500101n | J. Chem. Inf. Model. XXXX, XXX, XXX−XXX

The more intense rigid motion of the second p75NTR chain might be compatible with its easier dissociation from the proNGF.

The 2:1 complex formed by the mature NGF (Figure 9) has one single p75NTR chain binding both to the upper binding site (close to L2) and to the lower one (at L3) of the same NGF monomer. According to the Essential Dynamics analysis, during MD in the 2:1 complex, the p75NTR chain explores different orientations of its N-terminal part close to loop L2 and binding Site 1 of its NGF moiety. This behavior is similar to the one observed for the first p75NTR (chain X) bound to the proNGF dimer. In particular, the absence of significant collective motions at the C-terminal end of p75NTR that contacts binding Site 2 and loop L3 shows that the dynamics of this chain differs from the second monomer (chain Y) bound in the 2:2 complex. The local flexibility analysis in the previous section suggested that, in the absence of p75NTR, the main local mobility is localized either at loop L2 or at loop L3 in the loops "open" (proNGF) or loops "closed" state (mature NGF), respectively. It can be inferred also from this analysis that the binding of the receptor creates an intermediate state with local flexibility distributed at both regions. In the 2:2 complex, loops L2 are rather mobile already in the unbound NGF dimer (Figure 8A). However, upon binding, their motion becomes more ordered, and one of them evolves toward a conformation resembling the mature loops "open" state. The other one, which is bound to the second p75NTR (chain Y), is stably oriented in a perpendicular direction.

In the 2:1 complex (Figures 8A, 10B), we see that loop L2 contacting the p75NTR chain slightly increases its motion. The associated dynamical effect is propagated and magnified at the facing L2 from chain B, whose evolution during MD is toward a more open state. Interestingly, also the dynamics of the free L3 on chain B, located downstream from L2 and far away from the p75NTR interacting partner, undergoes a strong collective motion. This corresponds to the transition from the starting, exposed wing-like conformation to a more collapsed structure, similar to the receptor bound L3. In order to check that the collective dynamical behavior we observe in all trajectories is an equilibrium feature of the system and is not due to a single event, we repeated the PCA analysis on the two separated halves of the trajectory, corresponding to time intervals 5−50 ns and 50−100 ns. The convergence of the simulations was checked by considering the overlap of the essential subspaces resulting from the PCA analysis on the two halves. The overlap was calculated by means of the RMSIP measure (see Methods) yielding high values in all cases, indicating an overall significant convergence. In particular, the RMSIP value is 0.82 for the isolated proNGF, 0.75 for the isolated mature NGF, 0.86 for the 2:2 complex, and finally 0.79 for the 2:1 complex. For the last one, in particular, we verified that the coupled motion of loop L3 and of loop L2 is present in the first essential eigenvector in both trajectory halves (Figures S9 and S10). Hence, we can conclude that in the 2:1 complex the unbound NGF moiety appears to reflect in an allosteric manner the presence of the p75NTR chain binding to its dimer partner, by activating a collective motion.

3.2.2. Correlated Motions between Loops L2, L3, and L4 in the Interconversion between Mature and Pro NGF. Prompted by the observation of a collective motion activated in mature NGF by the presence of one bound receptor, here we analyze the linear correlation between C alpha atom pairs within each NGF moiety to investigate coordinated motions and allosteric effects possibly occurring between L2 and L3 as well as L4 loop regions. We are particularly interested in relating our MD trajectories to a possible interconversion between loops "open" proNGF and loops "closed" in mature NGF. In principle, such interconversion might occur spontaneously in the isolated NGF dimer or might be facilitated by the presence of the bound receptor. In order to describe this transition, we calculated the covariance matrix built considering the two crystal structures, as the extremes of the motion. This offers a simplified model of the structural transition, which however highlights the anticorrelation between the motion of loops L3 and L2 (Figure S11). Thereby, the structural transition of each L2 is anticorrelated not only to the corresponding L2 from the other monomer but also to the L3 belonging to the same chain. This means that, whereas one loop L2 goes outward transitioning from the mature to the proNGF state, the corresponding L3 is moving inward and at the same time the L2 of the facing monomer is going outward too. Keeping this anticorrelation pattern in mind, we evaluate the linear correlation by looking at the reduced covariance matrix obtained for NGF and proNGF dimers in all MD trajectories, both in the isolated and in the p75NTR bound state. Here we focus on the internal correlation of NGF dimers, which was calculated after aligning the trajectories on the starting conformation of the NGF dimer, while the reduced covariance matrix of the whole complexes (considering also the receptor in the fitting as done in the previous section) is shown in the Supporting Information.

The linear correlation matrices of the unbound pro- and mature NGF constructs show an overall mild positive correlation and significant values within L2 and L3, respectively, but no coupling between them, as expected (Figures 10A, 10C, 10D). Similarly, in the proNGF bound to two p75NTR chains, the covariance maintains the same features it has in the unbound proNGF dimer, with correlated motion limited to L2. On the other hand, the 2:1 complex formed by the mature NGF (Figure 10B) shows, in agreement with the previous results, an increase of (anti) correlated motion between L2 and L3 of the NGF monomer not bound to p75NTR, which resembles the pattern characterizing the interconversion between loops "closed" and loops "open" state (Figure S12). This suggests that the L2−L2 interaction characterizing the mature NGF state can be perturbed by the p75NTR chain interacting with one L2 on one side. This increases the motion of the other L2 loop, and one can speculate that this motion might facilitate the separation of the loops and eventually lead to the conversion into the loops "open" state. Also, the motion of loops L2 is accompanied by the anticorrelated motion of loop L3.

Interestingly, in both systems the presence of the p75NTR receptor induces a higher internal rigidity and therefore smaller fluctuations along and close to the diagonal in the mature and proNGF dimers relative to the unbound state. This can be expected due to the coordinating effect of the rigid receptor connecting the extremes of the NGF molecule. However, the fitting on the NGF dimer highlights an overall similar distribution of correlation patterns in all cases.

DISCUSSION AND CONCLUSION

In this work, we addressed important structural and energetic factors that regulate the stoichiometry of NGF/p75NTR and proNGF/p75NTR complexes. Although both crystal structures are known, the dynamics of their association has remained

dx.doi.org/10.1021/ci500101n | J. Chem. Inf. Model. XXXX, XXX, XXX−XXX

elusive. To address this issue we focused our attention on (i) the stability of the different stoichiometries; (ii) the importance of the structural rearrangement of the loops; and (iii) the role of the receptor binding in the conformational rearrangement of the neurotrophins. Mature neurotrophins bound to p75NTR crystals have shown different binding stoichiometries with the mature NGF molecule bound to one p75NTR ectodomain (2:1) and the mature neurotrophin-3 bound to two p75NTR ectodomains (2:2). For the proNGF/p75NTR complex, 2:2 and 2:1 stoichiometries were also shown to exist. A structural comprehension of this range of stoichiometries for NGF/p75NTR complexes is still missing. Here, by performing MD simulations and a variety of structural/energetic analysis, we showed that the 2:2 proNGF/p75NTR is not a symmetrical complex. From the dynamical point of view the p75NTR chains show an asymmetric behavior, in that only one chain has increased mobility, highlighted by the Essential Dynamics analysis. This asymmetry might be the consequence of a looser binding of one chain relative to the other and possibly result in its unbinding. Hence, our findings are compatible with a scenario in which the 2:1 stoichiometry for the proNGF/p75NTR complex is in equilibrium with the 2:2 via asymmetric unbinding of one single p75NTR chain. Therefore, it is possible to infer that the complex with a 2:2 stoichiometry (proNGF/p75NTR) might be an intermediate form previous to the formation of a 2:1 complex able to bind to the receptor sortilin and activate the cell death pathway. As an important caveat, we have to stress the intrinsic limitations of exploring the conformational dynamics of the complex on a short time interval, which also affect the PCA. Our findings are nevertheless supported by the experimental observation of asymmetric B factors for the two p75NTR chains in the crystal structure of the 2:2 complex.

In the mature NGF complex, we have also observed an increase of the (anti) correlated motion between L2 and L3 of the monomer not directly bound to the receptor, characteristic of an interconversion between loops "closed" and loops "open". The same caveat formulated above on the limitation of our MD sampling and Essential Dynamics analysis applies here. In particular, the loop motions have lifetimes comparable to the length of MD simulations, which prevents us from showing conclusive evidence. Yet, based on the local flexibility analysis, we can hypothesize that in the 2:1 form, one of the NGF monomers might be able to strongly increase its loop motion and possibly even convert to an "open" state that mimics the one observed for the pro-form. This hypothesis deserves further experimental investigation, since it is highly relevant and could explain the dual role of the mature NGF in nervous system development, where it has been shown to have antagonistic effects promoting either neuronal survival or apoptosis.[53,54]

We also showed that the mature NGF presents 12 HS with an average binding affinity of 3.77 kcal/mol. For the proNGF bound to chain X, we found 10 HS with an average of 4.29 kcal/mol. The results are in agreement with the experimental data, which have shown the existence of higher-affinity binding to a few sites in the proNGF, whereas mature NGF exhibited lower-affinity binding to many sites.[6] Given the observed effects of the neurotrophins structure over the overall complex, a more in depth study of the interactions between NGF chains as well as their structural stability and movement was proven necessary. The proNGF/p75NTR complex has more HS involved not only in the stability of the p75NTR chain X but also in binding of the neurotrophin dimer itself, which justifies the greater stability of chains A and B of the NT when compared with the mature NGF/p75NTR complex (Figure S1). It is also noticeable that there is a greater "symmetry" of the HS (same residues as HS in chain A and B) for the complexes with proNGF. The reason for these findings might be the different spatial orientation of the NGF chains for NGF/p75NTR in comparison with their parallel orientation in the proNGF/p75NTR complex. Previous works have pointed out that the NGF chains are canted in the mature dimer and proposed that this was the result of the p75NTR binding in an asymmetric mode.[3]

MD simulations of the neurotrophin dimers alone in solution were performed to study the structural and stability effects of the neurotrophin dimers binding to the receptor p75NTR. The NGF dimer shows a different behavior between the two complexes. Upon p75NTR binding to NGF, the stability of the dimer is increased, and one of the NGF chains presents a lower fluctuation, which is explained by the higher number of hot-spots in the NGF/p75NTR interface. Opposite to this behavior, the dimer with its pro-form does not show significant differences in chain stability. Both chains were very stable during the MD simulation with the exception of a specific time interval (40−60 ns). Without the presence of the receptor molecule and with L2 in an "open" state, there is a decrease of the distance between L4s. Therefore, unlike the mature NGF dimer, we have not observed any steric clashes between L2 and L4. However, no changes in "closed"/"open" states of the loops occurred. As seen in the projection of the eigenvectors the movement on the loops is a concerted movement involving both L2 partners, which explains why the distances between them remain stable for the most part. Although the stability and binding of p75NTR present different behaviors among the analyzed complexes, it is possible to characterize p75NTR chains' movement as seen in the projection of the eigenvectors. The center of these chains is the most stable part of the molecule, while both extremities present a "crab-like" movement as previously described.[6]

The comprehensive analyses of the behavior of mature NGF/proNGF alone upon binding to p75NTR have also shown that the structure of the neurotrophins is not rigid. Although NGF chains present a well-defined and stable overall structure, it became clear that structural differences occur upon receptor binding. These differences could be the basis of different higher order molecular complexes. Our hypothesis that the 2:2 proNGF/p75NTR complex is transient and rapidly gives rise to a 2:1 complex would imply that upon binding of proNGF to p75NTR an open side is created by unbinding of a p75NTR chain, opening the possibility that sortilin could be recruited forming a heterotrimeric complex. In fact, it is tempting to think that such structural organization could promote a conformation change in the intracellular domain (ICD) of p75NTR known to be responsible for the recruitment of adaptor proteins, which initiate the death cascade.[54] These results shed new light in the opposite biological actions of neurotrophins (neurotrophic vs apoptotic) with specific ligands, inducing diverse complex stoichiometries and/or different tertiary structures to recruit singular intracellular signaling partners. Moreover, neurotrophins are known modulators of neuronal injury like ischemia, excitotoxicity, and spinal cord lesions,[13,55,56] and their levels altered in several neuronal disorders like Alzheimer's disease, epilepsy, schizophrenia, learning, and memory.[57] Successful approaches to modulate this system are still missing. Initial clinical trials with

neurotrophins revealed disappointing results and were suspended.[58] However, recent studies have reported interesting findings using small-molecule ligands.[59−63] Although this strategy requires additional studies to overcome specificity and side effect problems, it is currently a promising approach to relaunch neurotrophins as a therapeutic approach.[53] In line with these studies and from a biomedical point of view, our results can provide new perspectives for the development of novel pharmacological tools to modulate ligand−receptor interactions and as a consequence neurotrophin related diseases.

■ ASSOCIATED CONTENT

Supporting Information

The Supporting Information is comprised of 12 figures and 9 tables. Figure S1: RMSD plots of the backbone of the different chains composing both complexes as well as complete systems. (A) NGF/p75NTR and (B) proNGF/p75NTR complexes; Figure S2: RMSD plots of the backbone of the different chains composing both complexes as well as complete systems. (A) NGF and (B) proNGF dimers; Figure S3: RMSD plots of the backbone of the structured motifs (β-sheets and α-helices) and loops of the studied systems. (A) pro NGF/p75NTR, (B) the proNGF dimer, (C) NGF/p75NTR, (D) the NGF dimer; Figure S4: Graphical representation of the relative free binding energy of all residues detected as HS for the NGF/NGF dimer: mature NGF (A) and proNGF (B) complexes, respectively; Figure S5: Average ΔSASA for the HS and NS of the fours systems in study; Figure S6: Average RMSF for the HS and NS of all four systems; Figure S7: RMSF values for the four systems in study. HS are in an orange if influence the NGF/p75NTR interface, blue if influence the NGF/NGF interface, and in yellow if they are important for both types of interfaces; Figure S8: Local flexibility along the p75NTR chain; Figure S9: Correlation analysis of motions of NGF in the mature complex. A) reduced covariance matrix over the first 50 ns; B) reduced covariance matrix over the second half of the trajectory; C) extreme conformations along the first essential eigenvector for the first half of the trajectory; D) extreme conformations along the first essential eigenvector for the second half of the trajectory; Figure S10: Reduced covariance matrices obtained on two separate halves (First half: 5−50 ns; Second half: 50−100 ns) of each MD trajectory. A,B First and second half of isolated mature NGF. C,D First and second half of isolated proNGF. E,F First and second half of proNGF in complex with 2 receptor chains; Figure S11: Covariance matrix describing the structural transition between proNGF and mature NGF. Loops L2 (residues 40−50) and L3 (residues 60−70) are anticorrelated; Figure S12: Covariance matrix obtained from MD simulations of the mature NGF + one p75NTR chain (A) and pro NGF + two p75NTR chains; Table S1: Decomposition of the relative binding free energy upon computational ASM for the complex mature NGF/p75NTR. The residues with $\Delta\Delta G_{binding}$ within the experimental error were colored in blue and the ones outside this error were colored in green. Experimental values are listed within brackets; Table S2: Decomposition of the relative binding free energy upon computational ASM for the complex proNGF/p75NTR; Table S3: H-bonds and salt-bridge information involving the HS at the mature NGF/p75NTR. Lifetime is a measure of the average time the interaction is formed. Only interactions pairs with occupancy higher than 30% are shown. In orange are colored the residues involved in the mature NGF/p75NTR interface, in blue the residues involved in the NGF/NGF interface, and in yellow are represented the residues common in both interfaces; Table S4: Alanine shaving results for the mature NGF/p75 complex. In orange are colored the residues involved in the mature NGF/p75NTR interface, in blue the residues involved in the NGF/NGF interface, and in yellow are represented the residues common in both interfaces; Table S5: H-bonds and salt-bridge information for the proNGF/p75NTR. Lifetime is a measure of the average time the interaction is formed. Only interactions pairs with occupancy higher than 30% are shown. In orange are colored the residues involved in the proNGF/p75NTR interface, in blue the residues involved in the proNGF/proNGF interface, and in yellow are represented the residues common in both interfaces; Table S6: Alanine shaving results for the proNGF/p75 complex. In orange are colored the residues involved in the proNGF/p75NTR interface and in yellow are represented the residues common in both interfaces; Table S7: Decomposition of the relative binding free energy upon computational ASM for the dimer NGF/NGF; Table S8: Decomposition of the relative binding free energy upon computational ASM for the complex proNGF/proNGF; Table S9: H-bonds and salt-bridge information for the mature NGF dimer. Lifetime is a measure of the average time the interaction is formed. Only interactions pairs with occupancy higher than 30% are shown; Table S10: Alanine shaving results for the dimers. We have colored in orange the residues involved in the proNGF/pro NGF interface and yellow the ones involved in the mature one. This material is available free of charge via the Internet at http://pubs.acs.org.

■ AUTHOR INFORMATION

Corresponding Author

*E-mail: irina.moreira@fc.up.pt.

Notes

The authors declare no competing financial interest.

■ ACKNOWLEDGMENTS

I.S.M. is supported by FCT Ciência 2008 (Hiring of PhDs for the SCTN - financed by POPH - QREN - Typology 4.2 - Promoting Scientific Employment, cofinanced by MES national funding and The European Social Fund). D.F.A.R. gratefully acknowledges salary support from Uppsala University, Department of Cell and Molecular Biology - Computational and Systems Biology and computational resources from High Performance Computing Center North (HPC2N). R.D.A is supported by FEDER through COMPETE and by FCT (PTDC/SAU-NEU/104100/2008; PEst-C/SAU/LA0001/2013-2014) and by Marie Curie Actions, seventh Framework Programme, EU. This work has been further supported by FCT through grant no. PEst-/EQB/LA0006/2011.

■ REFERENCES

(1) Wiesmann, C.; Fau - de Vos, A. M.; de Vos, A. M. Nerve growth factor: structure and function. *Cell. Mol. Life Sci.* **2001**, *58*, 748−759.

(2) Snider, W. D. Functions of the neurotrophins during nervous system development: What the knockouts are teaching us. *Cell* **1994**, *77*, 627−638.

(3) He, X. L.; Garcia, K. C. Structure of nerve growth factor complexed with the shared neurotrophin receptor p75. *Science* **2004**, *304*, 870−875.

(4) Paoletti, F.; Malerba, F.; Kelly, G.; Noinville, S.; Lamba, D.; Cattaneo, A.; Pastore, A. Conformational plasticity of proNGF. *PLoS One* **2011**, *6*, e22615.

(5) Teng, K. K.; Hempstead, B. L. Neurotrophins and their receptors: signaling trios in complex biological systems. *Cell. Mol. Life Sci.* **2004**, *61*, 35−48.
(6) Feng, D.; Kim, T.; Ozkan, E.; Light, M.; Torkin, R.; Teng, K. K.; Hempstead, B. L.; Garcia, K. C. Molecular and structural insight into proNGF engagement of p75NTR and sortilin. *J. Mol. Biol.* **2010**, *396*, 967−984.
(7) Rattenholl, A.; Ruoppolo, M.; Flagiello, A.; Monti, M.; Vinci, F.; Marino, G.; Lilie, H.; Schwarz, E.; Rudolph, R. Pro-sequence assisted folding and disulfide bond formation of human nerve growth factor. *J. Mol. Biol.* **2001**, *305*, 523−533.
(8) Rattenholl, A.; Lilie, H.; Grossmann, A.; Stern, A.; Schwarz, E.; Rudolph, R. The pro-sequence facilitates folding of human nerve growth factor from Escherichia coli inclusion bodies. *Eur. J. Biochem.* **2001**, *268*, 3296−3303.
(9) Chen, L. W.; Yung, K. K.; Chan, Y. S.; Shum, D. K.; Bolam, J. P. The proNGF-p75NTR-sortilin signalling complex as new target for the therapeutic treatment of Parkinson's disease. *CNS Neurol. Disord.: Drug Targets* **2008**, *7*, 512−523.
(10) Shooter, E. M. Early Days of the Nerve Growth Factor Proteins. *Annu. Rev. Neurosci.* **2001**, *24*, 601−629.
(11) Kliemannel, M.; Golbik, R.; Rudolph, R.; Schwarz, E.; Lilie, H. The pro-peptide of proNGF: structure formation and intramolecular association with NGF. *Protein Sci.* **2007**, *16*, 411−419.
(12) Lee, R.; Kermani, P.; Teng, K. K.; Hempstead, B. L. Regulation of cell survival by secreted proneurotrophins. *Science* **2001**, *294*, 1945−198.
(13) Harrington, A. W.; Leiner, B.; Blechschmitt, C.; Arevalo, J. C.; Lee, R.; Mörl, K.; Meyer, M.; Hempstead, B. L.; Yoon, S. O.; Giehl, K. M. Secreted proNGF is a pathophysiological death-inducing ligand after adult CNS injury. *Proc. Natl. Acad. Sci. U. S. A.* **2004**, *101*, 6226−6230.
(14) Nykjaer, A.; Lee, R.; Teng, K. K.; Jansen, P.; Madsen, P.; Nielsen, M. S.; Jacobsen, C.; Kliemannel, M.; Schwarz, E.; Willnow, T. E.; Hempstead, B. L.; Petersen, C. M. Sortilin is essential for proNGF-induced neuronal cell death. *Nature* **2004**, *427*, 843−848.
(15) Gong, Y.; Cao, P.; Yu, H. J.; Jiang, T. Crystal structure of the neurotrophin-3 and p75NTR symmetrical complex. *Nature* **2008**, *454*, 789−793.
(16) Eswar, N.; Webb, B.; Marti-Renom, M. A.; Madhusudhan, M. S.; Eramian, D.; Shen, M. Y.; Pieper, U.; Sali, A. Comparative protein structure modeling using MODELLER. *Curr. Protoc. Protein Sci.* **2007**, Chapter 2, Unit 2.9.
(17) Eswar, N.; Eramian, D.; Webb, B.; Shen, M. Y.; Sali, A. Protein structure modeling with MODELLER. *Methods Mol. Biol.* **2008**, *426*, 145−159.
(18) Bas, D. C.; Rogers, D. M.; Jensen, J. H. Very fast prediction and rationalization of pKa values for protein−ligand complexes. *Proteins: Struct., Funct., Bioinf.* **2008**, *73*, 765−783.
(19) Olsson, M. H. M.; Søndergaard, C. R.; Rostkowski, M.; Jensen, J. H. PROPKA3: Consistent Treatment of Internal and Surface Residues in Empirical pKa Predictions. *J. Chem. Theory Comput.* **2011**, *7*, 525−537.
(20) Søndergaard, C. R.; Olsson, M. H. M.; Rostkowski, M.; Jensen, J. H. Improved Treatment of Ligands and Coupling Effects in Empirical Calculation and Rationalization of pKa Values. *J. Chem. Theory Comput.* **2011**, *7*, 2284−2295.
(21) Li, H.; Robertson, A. D.; Jensen, J. H. Very fast empirical prediction and rationalization of protein pKa values. *Proteins: Struct., Funct., Bioinf.* **2005**, *61*, 704−721.
(22) Berendsen, H.; Postma, J. P. M.; van Gunsteren, W. F. *Intermolecular Forces*; D. Reidel Publishing Company: Dordrecht, 1981; pp 331−342.
(23) Bussi, G.; Donadio, D.; Parrinello, M. Canonical sampling through velocity rescaling. *J. Chem. Phys.* **2007**, *126*, 014101.
(24) Parrinello, M.; Rahman, A. Polymorphic Transitions in Single-Crystals - a New Molecular-Dynamics Method. *J. Appl. Phys.* **1981**, *52*, 7182−7190.
(25) Essmann, U.; Perera, L.; Berkowitz, M. L.; Darden, T.; Lee, H.; Pedersen, L. G. A Smooth Particle Mesh Ewald Method. *J. Chem. Phys.* **1995**, *103*, 8577−8593.
(26) Hess, B.; Bekker, H.; Berendsen, H.; Fraaije, J. LINCS: A Linear Constraint Solver for molecular simulations. *J. Comput. Chem.* **1997**, *18*, 1463−1472.
(27) Lindahl, E.; Hess, B.; van der Spoel, D. GROMACS 3.0: A package for molecular simulation and trajectory analysis. *J. Mol. Model.* **2001**, *7*, 306−317.
(28) Wang, J.; Wolf, R. M.; Caldwell, J. W.; Kollman, P. A.; Case, D. A. Development and testing of a general amber force field. *J. Comput. Chem.* **2004**, *25*, 1157−1174.
(29) Sorin, E. J.; Pande, V. S. Exploring the helix-coil transition via all-atom equilibrium ensemble simulations. *Biophys. J.* **2005**, *88*, 2472−2493.
(30) Cornell, W. D.; Cieplak, P.; Bayly, C. I.; Gould, I. R.; Merz, K. M., Jr.; Ferguson, D. M.; Spellmeyer, D. C.; Fox, T.; Caldwell, J. W.; Kollman, P. A. A Second Generation Force Field for the Simulation of Proteins, Nucleic Acids, and Organic Molecules. *J. Am. Chem. Soc.* **1995**, *117*, 5179−5197.
(31) Krissinel, E.; Henrick, K. Inference of Macromolecular Assemblies from Crystalline State. *J. Mol. Biol.* **2007**, *372*, 774−797.
(32) Case, D. A.; Cheatham, T. E.; Darden, T.; Gohlke, H.; Luo, R.; Merz, K. M.; Onufriev, A.; Simmerling, C.; Wang, B.; Woods, R. J. The Amber biomolecular simulation programs. *J. Comput. Chem.* **2005**, *26*, 1668−88.
(33) Huo, S.; Massova, I.; Kollman, P. A. Computational alanine scanning of the 1:1 human growth hormone-receptor complex. *J. Comput. Chem.* **2002**, *23*, 15−27.
(34) Case, D. A.; Darden, T. A.; Cheatham, T. E.; Simmerling, C. L.; Wang, J.; Duke, R. E.; Luo, R.; Crowley, M.; Walker, R. C.; Zhang, W.; Merz, K. M.; Wang, B.; Hayik, S.; Roitberg, A.; Seabra, G.; Kolossváry, I.; Wong, K. F.; Paesani, F.; Vanicek, J.; Wu, X.; Brozell, S. R.; Steinbrecher, T.; Gohlke, H.; Yang, L.; Tan, C.; Mongan, J.; Hornak, V.; Cui, G.; Mathews, D. H.; Seetin, M. G.; Sagui, C.; Babin, V.; Kollman, P. A. AMBER 10; University of California: San Francisco, 2008.
(35) Moreira, I. S.; Fernandes, P. A.; Ramos, M. J. Computational alanine scanning mutagenesis - An improved methodological approach. *J. Comput. Chem.* **2007**, *28*, 644−654.
(36) Kollman, P. A.; Massova, I.; Reyes, C.; Kuhn, B.; Huo, S. H.; Chong, L.; Lee, M.; Lee, T.; Duan, Y.; Wang, W.; Donini, O.; Cieplak, P.; Srinivasan, J.; Case, D. A.; Cheatham, T. E. Calculating structures and free energies of complex molecules: Combining molecular mechanics and continuum models. *Acc. Chem. Res.* **2000**, *33*, 889−897.
(37) Rocchia, W.; Alexov, E.; Honig, B. Extending the applicability of the nonlinear Poisson-Boltzmann equation: Multiple dielectric constants and multivalent ions. *J. Phys. Chem. B* **2001**, *105*, 6507−6514.
(38) Rocchia, W.; Sridharan, S.; Nicholls, A.; Alexov, E.; Chiabrera, A.; Honig, B. Rapid grid-based construction of the molecular surface and the use of induced surface charge to calculate reaction field energies: Applications to the molecular systems and geometric objects. *J. Comput. Chem.* **2002**, *23*, 128−137.
(39) Moreira, I. S.; Fernandes, P. A.; Ramos, M. J. Accuracy of the numerical solution of the Poisson-Boltzmann equation. *J. Mol. Struct.: THEOCHEM* **2005**, *729*, 11−18.
(40) Sitkoff, D.; Sharp, K. A.; Honig, B. Accurate calculation of hydration free-energies using macroscopic solvent models. *J. Phys. Chem.* **1994**, *98*, 1978−1988.
(41) Moreira, I. S.; Fernandes, P. A.; Ramos, M. J. Unravelling Hot Spots: a comprehensive computational mutagenesis study. *Theor. Chem. Acc.* **2007**, *117*, 99−113.
(42) Connolly, M. L. Analytical molecular surface calculation. *J. Appl. Crystallogr.* **1983**, *16*, 548−558.
(43) Chen, C. Z.; Shapiro, R. Superadditive and subadditive effects of "hot spot" mutations within the interfaces of placental ribonuclease inhibitor with angiogenin and ribonuclease A. *Biochemistry* **1999**, *38*, 9273−9285.

(44) Lee, B.; Richards, F. M. The interpretation of protein structures: Estimation of static accessibility. *J. Mol. Biol.* **1971**, *55*, 379−400.
(45) Morra, G.; Potestio, R.; Micheletti, C.; Colombo, G. Corresponding functional dynamics across the Hsp90 Chaperone family: insights from a multiscale analysis of MD simulations. *PLoS Comput. Biol.* **2012**, *8*, e1002433.
(46) Hess, B.; Kutzner, C.; van der Spoel, D.; Lindahl, E. GROMACS 4: Algorithms for Highly Efficient, Load-Balanced, and Scalable Molecular Simulation. *J. Chem. Theory Comput.* **2008**, *4*, 435−447.
(47) Amadei, A.; Ceruso, M. A.; Di Nola, A. On the convergence of the conformational coordinates basis set obtained by the essential dynamics analysis of proteins' molecular dynamics simulations. *Proteins: Struct., Funct., Bioinf.* **1999**, *36*, 419−424.
(48) Spiliotopoulos, D.; Spitaleri, A.; Musco, G. Exploring PHD Fingers and H3K4me0 Interactions with Molecular Dynamics Simulations and Binding Free Energy Calculations: AIRE-PHD1, a Comparative Study. *PLoS One* **2012**, *7*, 36944−36955.
(49) Rydén, M.; Ibáñez, C. F. A Second Determinant of Binding to the p75 Neurotrophin Receptor Revealed by Alanine-scanning Mutagenesis of a Conserved Loop in Nerve Growth Factor. *J. Biol. Chem.* **1997**, *272*, 33085−33091.
(50) Moreira, I. S.; Martins, J. M.; Ramos, R. M.; Fernandes, P. A.; Ramos, M. J. Understanding the importance of the aromatic amino-acid residues as hot-spots. *Biochim. Biophys. Acta, Proteins Proteomics* **2013**, *1834*, 404−414.
(51) Martins, J. M.; Ramos, R. M.; Pimenta, A. C.; Moreira, I. S. Solvent-accessible surface area: How well can be applied to hot-spot detection? *Proteins: Struct., Funct., Bioinf.* **2013**, *82*, 479−490.
(52) Yogurtcgu, O. N.; Erdemli, S. B.; Nussinov, R.; Turkay, M.; Keskin, O. Restricted mobility of conserved residues in protein-protein interfaces in molecular simulations. *Biophys. J.* **2008**, *94*, 3475−3485.
(53) Longo, F. M.; Massa, S. M. Small-molecule modulation of neurotrophin receptors: a strategy for the treatment of neurological disease. *Nat. Rev. Drug Discovery* **2013**, *12*, 507−525.
(54) Almeida, R. D.; Duarte, C. p75NTR Processing and Signaling: Functional Role. In *Handbook of Neurotoxicity*; Kostrzewa, R., Ed.; Springer: New York, 2014; pp 1899−1923.
(55) Gomes, J. R.; Costa, J. T.; Melo, C. V.; Felizzi, F.; Monteiro, P.; Pinto, M. J.; Inácio, A. R.; Wieloch, T.; Almeida, R. D.; Grãos, M.; Duarte, C. B. Excitotoxicity downregulates TrkB.FL signaling and upregulates the neuroprotective truncated TrkB receptors in cultured hippocampal and striatal neurons. *J. Neurosci.* **2012**, *32*, 4610−4622.
(56) Almeida, R. D.; Manadas, B. J.; Melo, C. V.; Gomes, J. R.; Mendes, C. S.; Grãos, M. M.; Carvalho, R. F.; Carvalho, A. P.; Duarte, C. B. Neuroprotection by BDNF against glutamate-induced apoptotic cell death is mediated by ERK and PI3-kinase pathways. *Cell Death Differ.* **2005**, *12*, 1329−1343.
(57) Chao, M. V. Neurotrophins and their receptors: a convergence point for many signalling pathways. *Nat. Rev. Neurosci.* **2003**, *4*, 299−309.
(58) Thoenen, H.; Sendtner, M. Neurotrophins: from enthusiastic expectations through sobering experiences to rational therapeutic approaches. *Nat. Neurosci.* **2002**, *5* (Suppl), 1046−1050.
(59) Massa, S. M.; Xie, Y.; Yang, T.; Harrington, A. W.; Kim, M. L.; Yoon, S. O.; Kraemer, R.; Moore, L. A.; Hempstead, B. L.; Longo, F. M. Small, nonpeptide p75NTR ligands induce survival signaling and inhibit proNGF-induced death. *J. Neurosci.* **2006**, *26*, 5288−5300.
(60) Jang, S. W.; Liu, X.; Chan, C. B.; France, S. A.; Sayeed, I.; Tang, W.; Lin, X.; Xiao, G.; Andero, R.; Chang, Q.; Ressler, K. J.; Ye, K. Deoxygedunin, a natural product with potent neurotrophic activity in mice. *PLoS One* **2010**, *5*, e11528.
(61) Jang, S. W.; Liu, X.; Yepes, M.; Shepherd, K. R.; Miller, G. W.; Liu, Y.; Wilson, W. D.; Xiao, G.; Blanchi, B.; Sun, Y. E.; Ye, K. A selective TrkB agonist with potent neurotrophic activities by 7,8-dihydroxyflavone. *Proc. Natl. Acad. Sci. U. S. A.* **2010**, *107*, 2687−2692.
(62) Shin, S. B.; Almeida, R. D.; Gerona-Navarro, G.; Bracken, C.; Jaffrey, S. R. Assembling ligands in situ using bioorthogonal boronate ester synthesis. *Chem. Biol.* **2010**, *17*, 1171−1176.
(63) Baeza, J. L.; de la Torre, B. G.; Santiveri, C. M.; Almeida, R. D.; García-López, M. T.; Gerona-Navarro, G.; Jaffrey, S. R.; Jiménez, M.; Andreu, D.; González-Muñiz, R.; Martín-Martínez, M. Cyclic amino acid linkers stabilizing key loops of brain derived neurotrophic factor. *Bioorg. Med. Chem. Lett.* **2012**, *22*, 444−448.